An experimental parametric study on the liquefaction resistance of sands in spreader dumps of lignite opencast mines

T. Wichtmann[i] ; K. Steller[ii]; Th. Triantafyllidis[iii] ; M. Back[iv] ; D. Dahmen[v]

Abstract: The results of a parametric study on the liquefaction resistance of sands dumped with spreaders in lignite opencast mines using undrained cyclic triaxial tests is presented. Undisturbed samples taken by ground freezing and disturbed samples of the same material reconstituted by different methods were compared. Based on this comparison, a suitable sample preparation method was chosen which reproduces the depositional process in the dumps and leads to a similar initial fabric and thus a similar behaviour under undrained cyclic loading. Numerous tests on more than 50 sands from the dumps or the excavation sites of the mines demonstrated a decrease of the liquefaction resistance with increasing content of plastic fines and with decreasing mean grain size, while no clear trend with uniformity coefficient was observed in the data for a constant relative density. The dependence of the liquefaction resistance on the initial values of mean effective stress and stress ratio is discussed based on respective test series. Furthermore, the increase of the undrained cyclic strength with decreasing degree of saturation and an enhancement caused by a drained monotonic or vibrational preloading is demonstrated. Based on tests with different sample sizes, membrane penetration effects were found to be negligible.

Keywords: artificially deposited soils; lignite opencast mines; liquefaction resistance; cyclic triaxial tests; parametric study

1 Introduction

In lignite opencast mines the natural soil layers are excavated in order to reach the coal. The excavated soils are deposited on dumps lying either outside or inside the mines (see the photo of an example for an inner dump in Figure 1). The soils deposited in the dumps are somewhat artificial, since different natural soil layers may be mixed during the excavation and transportation process, due to the large dimensions of the shovels of the diggers compared to the thickness of the soil layers. Furthermore, the excavated soils are deposited in a moist state, usually falling from a certain height by using "spreaders" (Figure 1). The structure (fabric) of such deposited soils may significantly differ from that of natural soils. Deposited soils may contain a double porosity composed of micropores and macropores. Macropores are defined as pores with a size being larger than the mean grain size of the soil. They are stabilized by capillary effects at the grain contacts. Due to the different fabric and their rather loose state, knowledge regarding the mechanical behaviour of natural soils cannot be simply transferred to the artificially deposited soils in the dumps.

The experimental study presented in this paper is part of an ongoing research done in the laboratory of the Institute of Soil Mechanics and Rock Mechanics (IBF) at Karlsruhe

Fig. 1: *Dump site of lignite opencast mine Hambach, Germany*

[i]Professor for Geotechnical Engineering, Bauhaus-Universität Weimar, Germany (corresponding author). Email: torsten.wichtmann@uni-weimar.de

[ii]Researcher, Institute of Soil Mechanics and Rock Mechanics, Karlsruhe Institute of Technology, Germany

[iii]Professor and Director of the Institute of Soil Mechanics and Rock Mechanics, Karlsruhe Institute of Technology, Germany

[iv]RWE Power AG, Bergheim, Germany

[v]RWE Power AG, Bergheim, Germany

Institute of Technology (KIT). This research is dedicated to the soils deposited in the dumps of the opencast mines in the Rhenish lignite-mining area. After the depletion of the mines in several years to decades, the remaining holes of the currently three active mines Inden, Hambach and

Garzweiler will be recultivated as lakes. The deposited soils in the dumps will then form the embankment of these lakes. Since the Rhenish lignite-mining area lies in a region with seismic activity the liquefaction resistance of the deposited soils is of interest. The maximum moment magnitude M_W of earthquakes in the Lower Rhine Embayment based on palaeoseismic and tectonic studies has been estimated to 6.8-7.0 (e.g. [1, 36, 37]). Such strong earthquakes have return periods of several thousand years. Despite the existence of to date 57 mining lakes in this region, there was only one minor local effect of slope deformation, induced by the 1992 Roermond earthquake ($M_W = 5.4$, [12]) which was obviously not caused by liquefaction [84]. However, the embankments of the presently planned mining lakes are designed for the ground motion of an $M_W = 6$ earthquake with a typical number of equivalent cycles of $N_{eq} = 10$ and the corresponding distance from the epicenter of 5 km.

The following sections primarily document the experimental results regarding the liquefaction resistance of the deposited soils in the dumps of the Rhenish lignite-mining area. Since literature on the undrained cyclic behaviour of such artificially deposited soils is rare, several dependencies well-known for natural soils were inspected for the deposited soils. The laboratory testing program was accompanied by several field testing campaigns, primarily dedicated to the determination of the relative densities in the dumps.

2 Field testing

At different positions in the dumps of the lignite opencast mines samples were taken at the base of small pits excavated to a depth of about 2 m, either by means of large thin-walled tubes (diameter $d = 210$ mm, height $h = 260$ mm) or by ground freezing. From the blocks of frozen soil several triaxial samples ($d = h = 100$ mm) were cut out (see further explanations in Section 4). The material of the tube samples was mainly composed of sand. In some cases, however, it also contained some amount of clay lumps, pieces of coal or stones. All these particles with sizes larger than 10 mm were separated from the material of the tube samples by sieving. The mass and the volume of the oversized particles were subtracted from the total mass and total volume of the samples. With the remaining mass and volume the density of the sand matrix in the tube samples was calculated.

The water content w, the grain density ϱ_s and the minimum and maximum densities ($\varrho_{d,\min}, \varrho_{d,\max}$) or void ratios ($e_{\min}, e_{\max}$), respectively, were determined on subsamples. In case of the tube samples the subsamples were taken after separating the oversized particles. After completion of the triaxial tests all samples cut from the same frozen block were mixed with the remaining material of that block, before a subsample for index testing was gathered. According to German standard code DIN 18126 the minimum density was determined by loose placement of the oven-dried material in a cylinder by means of a funnel, while the maximum density was obtained from layerwise compaction under water. Conglomerates of grains cemented by the plastic fines during oven-drying of the material had to be carefully fractured before these index tests. With the void ratio e of a sample relative density was calculated from $D_r = (e_{\max} - e)/(e_{\max} - e_{\min})$.

The relative densities encountered in the different types of samples collected during several field campaigns are shown in the bar chart in Figure 2. They lie in the range $0\ \% \leq D_r \leq 67\ \%$, with average values of the individual sampling campaigns between 24 % and 42 %. The relative densities in the laboratory tests documented in the following sections were thus chosen in a similar range.
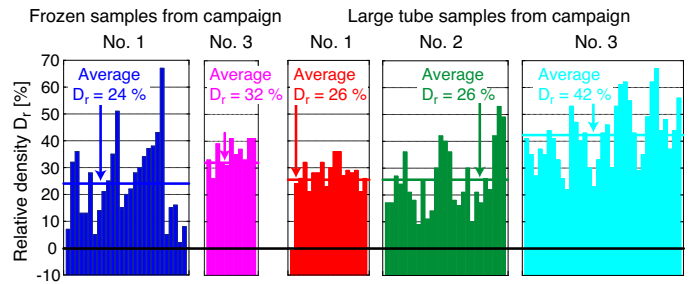
Fig. 2: *Relative densities D_r encountered in large tube samples ($d = 210$ mm, $h = 260$ mm) or triaxial samples ($d = h = 100$ mm) cut from larger undisturbed samples taken by ground freezing*

Furthermore, two large cones of moist soil were deposited by means of a spreader that is routinely used for the deposition on the dumps (Figure 3). Each cone had a height of about 11 m. One of these cones was excavated, taking about 80 large tube samples ($d = 210$ mm, $h = 260$ mm) along two orthogonal axes (in plane view) at different positions within the cone. The spatial distributions of relative density in the two cross sections are shown in Figure 4. Dynamic probings were performed along two orthogonal axes in the second cone. From both types of field investigations a rather uniform distribution of relative density in the deposited cones can be concluded, with an average value of again $D_r \approx 30$ %. The soil near the surface of the cones is somewhat looser. It would be further compacted, however, by the soil layers deposited above. The relative homogeneous distribution of relative density is probably a result of the large deformations of the soil within the cones, caused by the large kinetic energy of the spreaded soil mass striking the tip of the cone. The large deformations should approximately lead to a critical void ratio in the soil. During the field test it was observed that the spreaded soil masses do not role down along the surfaces of the cone, but penetrate the cone at its tip. Thus, during the depositional process the cone grows from the inside to the outside [94]. No compacted central column or tip as sometimes reported in the literature [16, 22, 51, 94] can be concluded from this field test.

The amount of macropores in the deposited soils was quantified indirectly by the measured settlement of undisturbed samples during water-saturation. The stabilizing capillary effects disappear during the saturation of the pore space with water and thus the macropores should collapse. Some of the large tube samples were directly flooded on the dump sites. Furthermore, the triaxial samples cut from the soil blocks taken by ground freezing were saturated in a triaxial device (Section 4). The maximum vertical strain during water-saturation measured for both types of samples was about 0.3 % only. Based on this low vertical strain, the amount of macropores in the deposited soils can be regarded as very small. This is probably the consequence of the large deformations occurring during the depositional process described above, leading to a strong reduction or

Fig. 3: *Deposition of two cones on the dump site of a lignite opencast mine by means of a spreader*

Fig. 4: *Distribution of relative density D_r in the two orthogonal cross sections of the deposited cone. The relative densities were determined based on the taken tube samples ($d = 210$ mm, $h = 260$ mm)*

even elimination of the macropores.

3   Influence of sample preparation method

For the parametric studies presented in the next sections a suitable sample preparation method reproducing the fabric of the deposited sands in the dumps had to be found. The large effect of the preparation method on the liquefaction resistance has been demonstrated by numerous researchers [31,59,60,68,71,72,83,86,102,103,109,111,112,117,135,137]. In a first step different sample preparation methods were compared for a typical sand from the dump site of a lignite opencast mine (material D1, fines content $FC = 5$ %, mean grain size $d_{50} = 0.51$ mm, uniformity coefficient $C_u = d_{60}/d_{10} = 3$, see grain size distribution curve in Figure 13 and parameters in Table 1). The fines content consists of a medium to highly plastic clay.

The samples (diameter $d = 100$ mm, height $h = 100$ mm in all tests of this study, except Section 11) were prepared

by four different methods (see Figure 5):

- Moist tamping in eight layers with the undercompaction method proposed by Ladd [61] (Figure 5a) using different degrees of undercompaction U (5, 10 and 15 %) and different water contents ($w = 5$, 7.5 and 10 %) during preparation.

- Free fall of moist material from a certain height out of a pipe into the split mould (Figure 5b). This procedure simulates the deposition technique in the dump sites of the opencast mines (Figures 1 and 3). Higher initial densities result from a higher falling height and/or a higher water content during preparation. Typical water contents during preparation lay in the range 5 % $\leq w \leq 20$ %.

- Deposition of a cone of moist sand by free fall (Figure 5c). Afterwards samples have been cut out in the vertical or horizontal direction by means of thin-walled stainless steel cylinders. The samples have been frozen in the cylinders. The frozen samples were dismantled from the cylinders, placed in the triaxial cell and thawed under small confining stresses. Using this method a possible influence of the wall of the split mould during the preparation by free fall as present in Figure 5b is prevented.

- Dry air pluviation (Figure 5d). This method was not thought to be realistic for the dumps in the opencast mines. However, as a common standard preparation method it was included in the present program. For that purpose the test material was dried. Conglomerates of the sand grains and the cohesive fines were carefully fractured before preparing the samples.

Fig. 5: *Applied sample preparation methods: a) Moist tamping, b) Free fall of moist material from a certain height H into the split mould, c) Sampling from a cone of moist sand deposited by the free fall method, d) Air pluviation*

If not otherwise stated the testing procedure was as described in the following in all triaxial tests of this study. After preparation the samples were set under an isotropic stress of $\sigma_1 = \sigma_3 = 50$ kPa. The pore space was first flushed with CO_2 and afterwards with demineralized deaerated water. The total stresses and the pore water pressure were then raised to $\sigma_1 = \sigma_3 = 220$ kPa and $u = 200$ kPa, respectively. Under these stresses the samples were again flushed

Fig. 6: Results of two tests on samples prepared either by moist tamping (a-d, with $U = 10$ % and $D_{r0} = 11$ %) or by taking a vertical sample out of a deposited cone of moist sand (e-h, with $D_{r0} = 49$ %): a,e) Development of total stresses with time, b,f) Development of axial strain with time, c,g) effective stress paths, d,h) stress-strain relationships

with demineralized deaerated water for some while. An increase of the stresses to $\sigma_1 = \sigma_3 = 520$ kPa and $u = 500$ kPa followed. After a resting period over night the degree of saturation was checked by means of the B value test. Usually B-values ≥ 0.99 were achieved. An isotropic effective stress with $p'_0 = 100$ kPa was used for all tests of this series. Therefore, the total stresses had to be increased to $\sigma_1 = \sigma_3 = 600$ kPa, keeping the back pressure at $u = 500$ kPa. After application of these initial stresses and a resting time of about 1 hour, the drainage was closed and the axial cyclic loading with a certain stress amplitude $\sigma_1^{\mathrm{ampl}} = q^{\mathrm{ampl}}$ was started. It was stopped when an axial strain of $|\varepsilon_1| = 10$ % (failure criterion) was reached.

Figure 6a-d shows typical test results for a loose sample ($D_{r0} = 11$ %) prepared by moist tamping ($w = 7.5$ %, $U = 10$ %) and loaded with a deviatoric stress amplitude $q^{\mathrm{ampl}} = 20$ kPa. Large extensional strains leading to failure ($|\varepsilon_1| = 10$ %) occur within a single cycle (Figure 6b), when the effective stress path (Figure 6c) comes close to the failure line in the extensional regime of the p'-q plane, known from monotonic triaxial extension tests. A typical behaviour for a denser sample ($D_{r0} = 49$ %) is shown in Figure 6e-h. This sample has been cut out of a deposited cone in the vertical direction (Figure 5c). A short phase of cyclic mobility at the end of the test is visible in the effective stress path (Figure 6g) and the stress-strain relationship (Figure 6h). In this test the failure criterion $|\varepsilon_1| = 10$ % has been fulfilled during triaxial compression (Figure 6f).

Figure 7 summarizes the results of tests on samples prepared by moist tamping with relative densities in the range 1 % $\leq D_{r0} \leq 28$ %. Different degrees of undercompaction ($U = 5$, 10 and 15 %) were used when preparing the samples with a water content of $w = 7.5$ %. For each U value, five tests with different amplitudes in the range 10 kPa

$\leq q^{\mathrm{ampl}} \leq 30$ kPa were performed, corresponding to cyclic stress ratios $0.05 \leq CSR = q^{\mathrm{ampl}}/(2p'_0) \leq 0.15$. In two additional tests the material was prepared with a lower ($w = 5$ %) or a higher water content ($w = 10$ %), using a degree of undercompaction of 5 %. The diagram in Figure 7 presents the cyclic stress ratio as a function of the number of cycles to failure ($|\varepsilon_1| = 10$ %). Certainly, this number decreases with increasing amplitude. Hardly any influence of the degree of undercompaction or the water content during preparation, however, can be concluded from the test data in Figure 7.
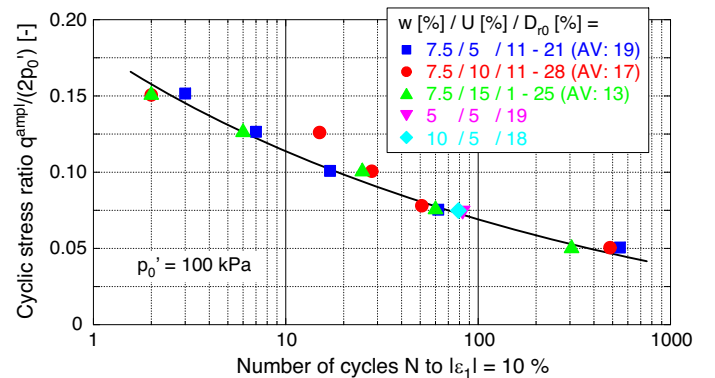
Fig. 7: Cyclic stress ratio $CSR = q^{\mathrm{ampl}}/(2p'_0)$ versus number of cycles N to failure for samples prepared by moist tamping using different degrees of undercompaction and water contents.

The CSR-N data for samples prepared by the three methods using moist material, i.e. moist tamping, free fall from a height of $H = 1.5$ m and vertical cutting out of a deposited cone (Figure 5a-c) are collected in Figure 8. The ranges of densities and in particular the average density was

similar for the three preparation methods. Despite some scatter, the data points and their best-fit curves in Figure 8 do not differ much between the three sample preparation methods.
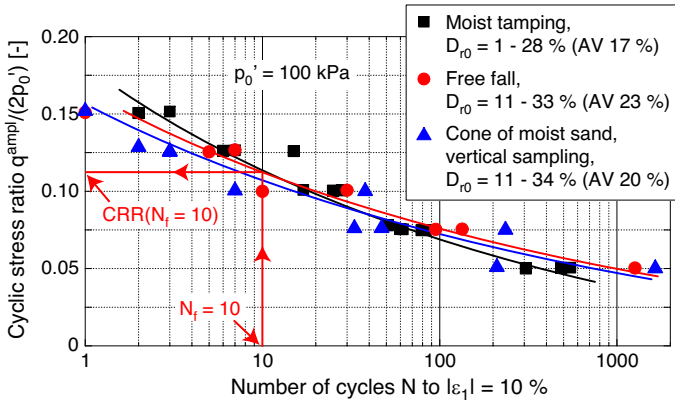
Fig. 8: *Cyclic stress ratio CSR versus number of cycles N to failure for samples prepared by moist tamping, free fall and vertical cutting out of a deposited cone. All samples have similar relative densities.*

From the curves in Figure 8 the liquefaction resistance $CRR(N_f = 10)$ (cyclic resistance ratio) was read as the cyclic stress ratio causing failure in $N_f = 10$ cycles. Additional test series with lower or higher densities (not shown in Figure 8) and other preparation methods (e.g. air pluviation) were included in the further analysis. In Figure 9 the $CRR(N_f = 10)$ values are plotted versus relative density D_{r0} measured before closure of drainage, showing an almost linear increase. In case of the deposited cones (Figure 5c) it is distinguished between vertical and horizontal samples and samples taken from either the center (only one sample) or the boundary (several samples) of the cone. From the data in Figure 9 it can be concluded that the liquefaction resistance is quite similar for all tested sample preparation methods. This applies even to the samples prepared by air pluviation. It is rather unimportant in which direction and at which position the samples were taken from the cones. Therefore, the anisotropy of the loose deposited sand seems to be negligible. The much simpler free fall method delivers similar $CRR(N_f = 10)$ values as the method were samples are taken from a deposited cone. Thus, the influence of the split mould on the fabric resulting from free fall seems to be small.

The rather small influence of the sample preparation method detected in the current study seems to contradict the literature. However, another study by the authors on sand C1 (Table 1) documented in [130] revealed a similar small effect at low relative densities. At medium density, however, the undrained cyclic strength of the samples prepared by moist tamping exceeded the one of their air-pluviated counterparts by far. The majority of the studies in the literature has been also performed on medium dense sand. Therefore, the effect of the sample preparation method on the liquefaction resistance seems to increase with growing density of the samples.
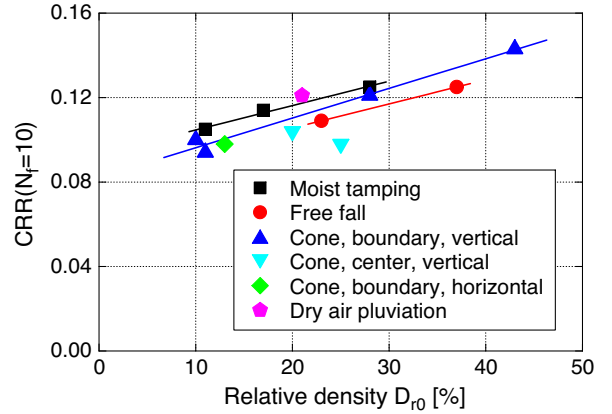
Fig. 9: *Liquefaction resistance $CRR(N_f = 10)$ (cyclic resistance ratio) as a function of relative density D_{r0} for different sample preparation methods*

4 Comparison of undisturbed samples taken by ground freezing and reconstituted samples

In a next step, undisturbed samples were taken on the dump site of a lignite opencast mine. At the ground of 10 small excavation pits with a depth of about 2 m the samples were obtained by ground freezing using liquid nitrogen. In total, 11 frozen soil blocks were sampled. Up to three triaxial samples were cut out of a frozen block in the laboratory. The procedure is shown in Figure 10. The results of index tests on the block materials resulted in the parameters summarized in Table 1 (materials F1 - F11). The frozen triaxial samples were built into the triaxial device. Thawing occurred under a low confining pressure of $p' = 50$ kPa. The undisturbed samples were tested at $p'_0 = 100$ kPa and with different amplitudes. Afterwards disturbed samples were prepared from the same material, using the methods of either free fall (falling height 1.5 or 2 m) or moist tamping in eight layers ($U = 10$ %). The reconstituted samples were prepared with similar densities as encountered in the undisturbed specimens. The aim of this study was to inspect if these artificial samples reflect the fabric of the deposited sand in the field. This is assumed to be the case if undisturbed and disturbed samples show the same behaviour.

In Figure 11 the effective stress paths and the stress-strain relationships measured for an undisturbed sample of sand F2 and two disturbed samples of the same material prepared by either free fall or moist tamping are compared. The samples were tested with the same amplitude $q^{ampl} = 25$ kPa. Despite some scatter in the initial relative densities, the overall material behaviour is quite similar for all three types of samples.

Figure 12 collects diagrams showing the liquefaction resistance $CRR(N_f = 10)$ in dependence of relative density D_{r0}, with data for the undisturbed and the disturbed samples. The values of mean grain size d_{50} and fines content FC of the sands are given in Figure 12 as well. The diagrams are ordered in a sequence with ascending values of d_{50} (the nomination of the sands from this sampling campaign in Table 1 has been chosen in the same way). The liquefaction resistance of the undisturbed samples and the disturbed samples prepared by free fall are quite similar for the finer sands F1 to F5 with low fines content (0.38 mm $\leq d_{50} \leq$ 0.43 mm, 0.8 % $\leq FC \leq$ 2.1 %) and also for the

Fig. 10: Preparation of triaxial samples ($d = h = 100$ mm) out of the frozen blocks
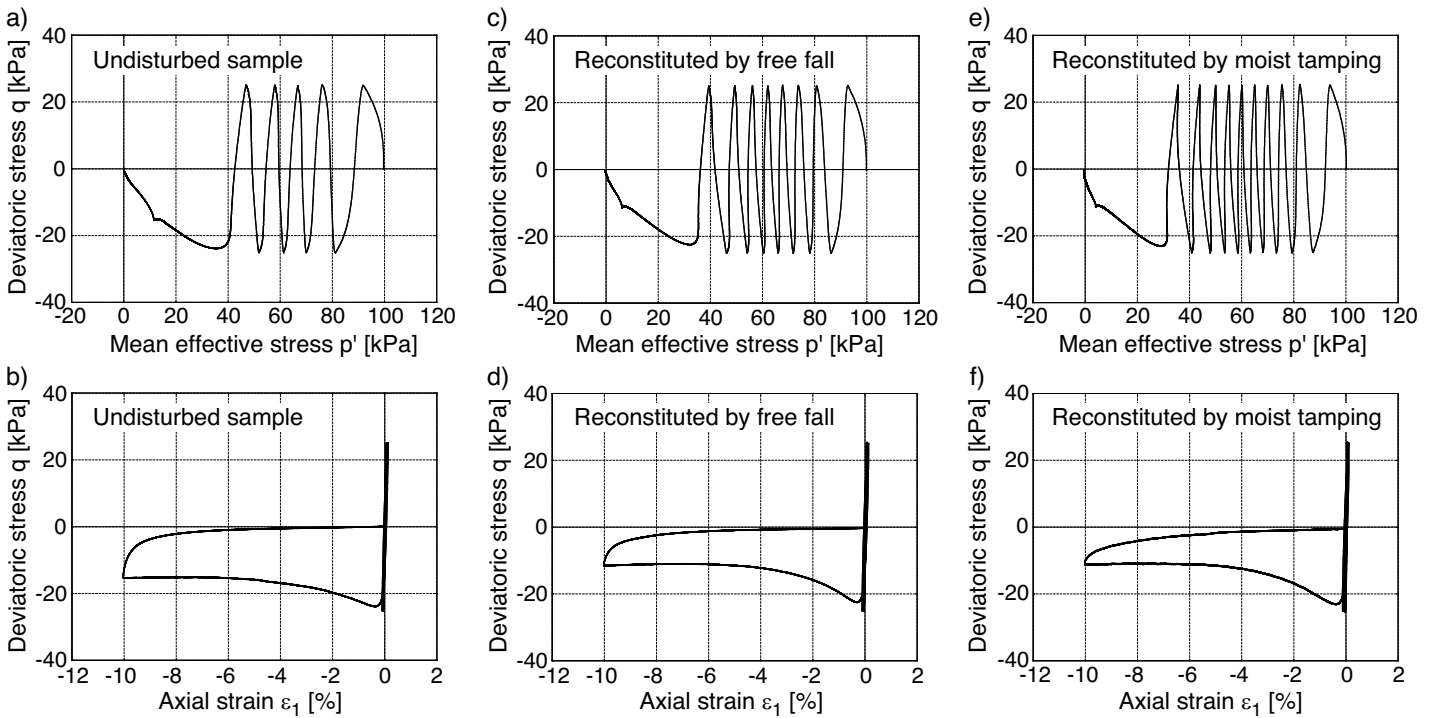
Fig. 11: *Effective stress paths and stress-strain relationships from undrained cyclic triaxial tests on sand F2: a) Undisturbed sample with $D_{r0} = 38$ %, b) Reconstituted sample prepared by free fall with $D_{r0} = 49$ %, c) Reconstituted sample prepared by moist tamping with $D_{r0} = 26$ %*

coarser sand F7 possessing a higher amount of fines ($d_{50} = 0.56$ mm, $FC = 4$ %). For those sands the disturbed samples prepared by moist tamping deliver a slightly higher undrained cyclic strength (see data for F1 and F2 in Figure 12). It is the other way around for the coarser materials F6 and F8 to F11 (0.51 mm $\leq d_{50} \leq 0.66$ mm, 0.8 % $\leq FC \leq 1.6$ %). For those materials the liquefaction resistance of the undisturbed samples is closer to that of the disturbed samples constituted by moist tamping, while the $CRR(N_f = 10)$ values of the artificial samples prepared by free fall lie somewhat below. Therefore, the method of free fall seems to better reproduce the soil fabric for finer sands or sands with higher fines contents, while the method of moist tamping is more suitable for coarser materials. However, the liquefaction resistance of the samples prepared by the free fall method is always equal or somewhat lower than that of the undisturbed samples. Therefore, this method of sample reconstitution seems to be conservative. It has thus been used for all further parametric studies.

In order to examine a possible effect of the preparation method in case of the undisturbed samples, in particular an influence of a possibly increased roughness of the surface of the trimmed sample, some special tests were performed on reconstituted samples of the soil F9. These samples were prepared with a larger geometry (diameter $d = 150$ mm, height $h = 150$ mm) by either free fall or moist tamping, before being frozen. Afterwards triaxial samples were cut out of the frozen cylinders using the same technique as in case of the undisturbed samples taken by ground freezing (Figure 10). These artificial samples showed a very similar behaviour in undrained cyclic triaxial tests, in particular a similar number of cycles to failure, as the disturbed samples of the same material prepared without freezing and trimming. Therefore, the method used to prepare the undisturbed triaxial samples out of the frozen blocks seems to have a negligible effect on the test results.

5 Influence of grain size distribution curve

The sands in the dumps of the lignite opencast mines possess a large bandwidth of grain size distribution curves. Therefore, the influence of the grain size distribution curve on the liquefaction resistance of the deposited soils has been
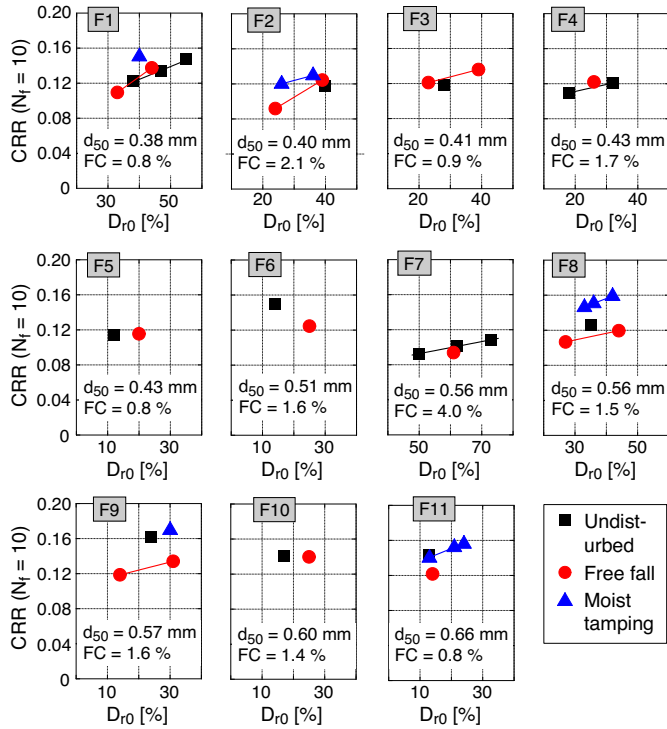
Fig. 12: *Comparison of the liquefaction resistance $CRR(N_f = 10)$ of undisturbed samples taken by ground freezing and reconstituted samples of the same material prepared by either free fall or moist tamping. Data for the sands F1 to F11*

inspected in a next step. The grain size distribution curves of the tested materials are shown in Figure 13 while their parameters are listed in Table 1. The 15 materials D1 to D15 were sampled on the dump sites of the opencast mines. 10 more materials (E1 to E10) were taken on the excavation sites of the mines. Three materials from the depositional site (D1-c to D3-c) and eight from the excavation site (E3-c to E10-c) were tested again after having washed out the fine material (fines content is defined by all grains with diameters < 0.063 mm according to German standard code [**?**]). Based on the fines separated from these sands, the fines content was classified as medium to highly plastic clay. Two more sands (DL1 and DL2) sampled on dump sites of the Lusation lignite mines in eastern Germany were also included in the program. Furthermore, two clean standard sands of the IBF (Karlsruhe fine sand and Karlsruhe sand) have been part of the testing program, denominated C1 and C2. An extensive experimental study on C1 is documented in [133, 134].

All samples were prepared by the free fall method. All materials were tested with different initial densities (varied by chosing different water contents and fall heights during preparation) and stress amplitudes. The initial mean effective stress was chosen as $p_0' = 100$ kPa in all tests of this series. Presentations of the test results in CSR-N diagrams looked similar to the data provided for sand D13 in Figure 17b. From such diagrams the liquefaction resistance $CRR(N_f = 10)$ for different relative densities D_{r0} was evaluated. The linear $CRR(N_f = 10)$-D_{r0} relationships for all sands are collected in Figure 14. Evidently, for a given relative density the liquefaction resistance strongly depends on the grain size distribution curve.

Material	FC [%]	d_{50} [mm]	C_u [-]	ϱ_s [g/cm³]	$\varrho_{d.\,min}$ [g/cm³]	$\varrho_{d.\,max}$ [g/cm³]
F1	0.8	0.42	1.8	2.64	1.381	1.698
F2	1.7	0.33	2.6	2.64	1.387	1.727
F3	0.9	0.41	1.8	2.63	1.400	1.715
F4	1.7	0.43	1.9	2.64	1.415	1.758
F5	0.8	0.43	1.9	2.64	1.415	1.746
F6	1.6	0.51	2.3	2.64	1.444	1.771
F7	4.0	0.57	5.8	2.64	1.487	1.881
F8	1.5	0.56	2.5	2.64	1.530	1.848
F9	1.6	0.57	2.2	2.64	1.466	1.775
F10	1.4	0.60	2.3	2.63	1.488	1.792
F11	0.8	0.66	2.2	2.64	1.515	1.795
D1	5	0.51	3.0	2.64	1.495	1.853
D2	14.7	0.14	2.6	2.63	1.289	1.650
D3	4.4	0.40	2.4	2.63	1.463	1.769
D4	6.4	0.56	3.6	2.66	1.605	1.936
D5	4.9	0.76	3.5	2.63	1.548	1.832
D6	5.2	0.45	2.7	2.64	1.464	1.774
D7	5.7	0.44	3.1	2.64	1.454	1.739
D8	4.2	0.43	2.1	2.63	1.413	1.682
D9	7.8	0.51	5.1	2.64	1.428	1.776
D10	5.6	0.16	2.3	2.64	1.272	1.628
D11	8.2	0.15	2.4	2.64	1.245	1.631
D12	10.2	0.54	10.3	2.64	1.483	1.832
D13	10.7	0.54	3.8	2.64	1.419	1.789
D14	3.0	0.42	1.8	2.64	1.431	1.699
D15	7.9	0.73	6.8	2.64	1.607	1.922
D1-c	0	0.50	2.6	2.64	1.493	1.803
D2-c	2.1	0.15	1.8	2.64	1.240	1.521
D3-c	0.3	0.43	2.3	2.64	1.451	1.779
E1	4.9	0.50	4.4	2.63	1.518	1.865
E2	4.8	0.69	1.9	2.64	1.514	1.866
E3	6.5	0.95	5.5	2.63	1.471	1.835
E4	5.0	0.40	2.9	2.64	1.425	1.757
E5	9.6	0.18	2.9	2.64	1.294	1.685
E6	4.9	0.25	2.1	2.64	1.324	1.681
E7	9.7	0.54	9.3	2.63	1.512	1.877
E8	3.1	0.45	2.0	2.64	1.444	1.779
E9	5.2	0.15	1.7	2.63	1.294	1.602
E10	3.3	0.34	2.0	2.63	1.431	1.725
E3-c	0.4	0.74	2.9	2.64	1.465	1.798
E4-c	0.2	0.41	2.3	2.64	1.427	1.762
E5-c	1.0	0.17	1.8	2.64	1.302	1.611
E6-c	0.4	0.27	1.7	2.64	1.317	1.625
E7-c	0.7	0.69	3.4	2.64	1.501	1.815
E8-c	0.4	0.39	1.9	2.64	1.426	1.732
E9-c	0.4	0.15	1.6	2.64	1.303	1.601
E10-c	0.5	0.36	2.0	2.64	1.443	1.764
DL1	0	0.39	2.3	2.64	1.546	1.853
DL2	17.7	0.17	3.8	2.64	1.456	1.908
C1	0.9	0.14	1.5	2.65	1.290	1.580
C2	0	0.56	1.5	2.64	1.427	1.705

Table 1: Fines content FC, mean grain size d_{50}, uniformity coefficient $C_u = d_{60}/d_{10}$, grain density ϱ_s and minimum and maximum dry densities $\varrho_{d,\min}$ and $\varrho_{d,\max}$ of the tested materials. In case of a fines content $10\ \% \leq FC \leq 20\ \%$, the uniformity coefficient was evaluated as $C_u^* = d_{70}/d_{20}$ due to missing information regarding the grain size distribution curve in the range $d < 0.063$ mm.

Fig. 13: *Grain size distribution curves of the tested materials*
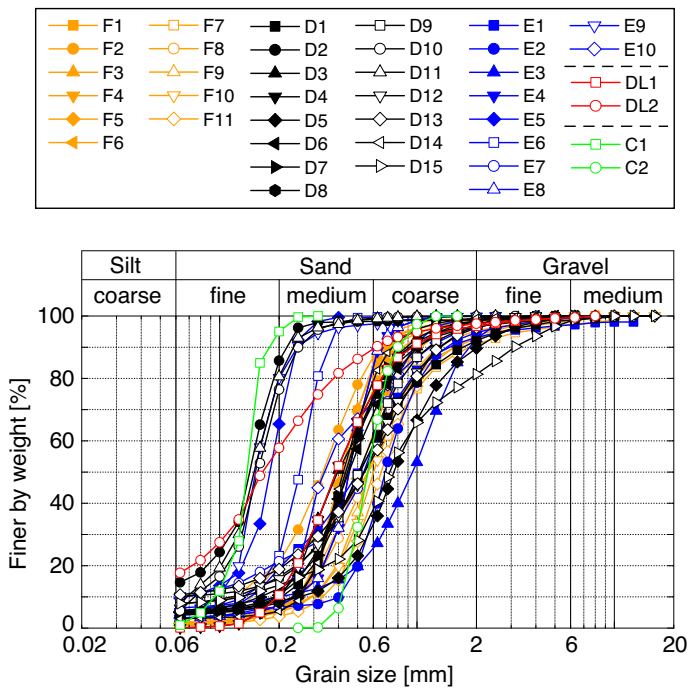
Fig. 14: *Liquefaction resistance $CRR(N_f = 10)$ in dependence of relative density D_{r0} for all tested materials*

Correlations between $CRR(N_f = 10)$ and the parameters of the grain size distribution curve have been further analyzed for a relative density of $D_{r0} = 30$ %. The liquefaction resistance $CRR(N_f = 10, D_{r0} = 30\%)$ was read from Figure 14 and plotted versus FC, d_{50} or C_u, respectively, in Figure 15. The data from the test series on the reconstituted samples of F1 to F11 documented in Section 4 are included in Figure 15. For a constant relative density, the liquefaction resistance tends to decrease with increasing fines content (Figure 15a, although the fines are plastic). While most of the research on the influence of fines was done on non-plastic fines (and is even contradictory in that case, see a literature review in [130]), much less information can be found in the literature regarding plastic fines. Cohesive fines are often reported to increase the liquefaction resistance of granular materials [15,32,42,43,47,58,87,117]. It is explained by the adhesion of the fines that hinder a separation of adjacent grains. However, in many cases the basis of comparison of the previous studies (i.e. constant void ratio, skeleton void ratio, equivalent void ratio or relative density) remains unclear. In partial agreement with some other researchers [82], the data from the current study show the opposite trend for the deposited soils.

Furthermore, the liquefaction resistance rises with mean grain size (Figure 15b), which is in accordance with the results of test series performed on natural sands [13,23,25, 63,95,97,117]. No clear trend with C_u can be concluded from the data in Figure 15c. This agrees with [3,53,123], while some other researchers found poorly graded soils to be more susceptible to liquefaction than well-graded ones [55,63,92,95]. A possible influence of membrane penetration effects on the liquefaction resistance, which gets larger with increasing grain size and may thus affect the relationship between $CRR(N_f = 10, D_{r0} = 30\%)$ and d_{50} is further inspected in Section 11.
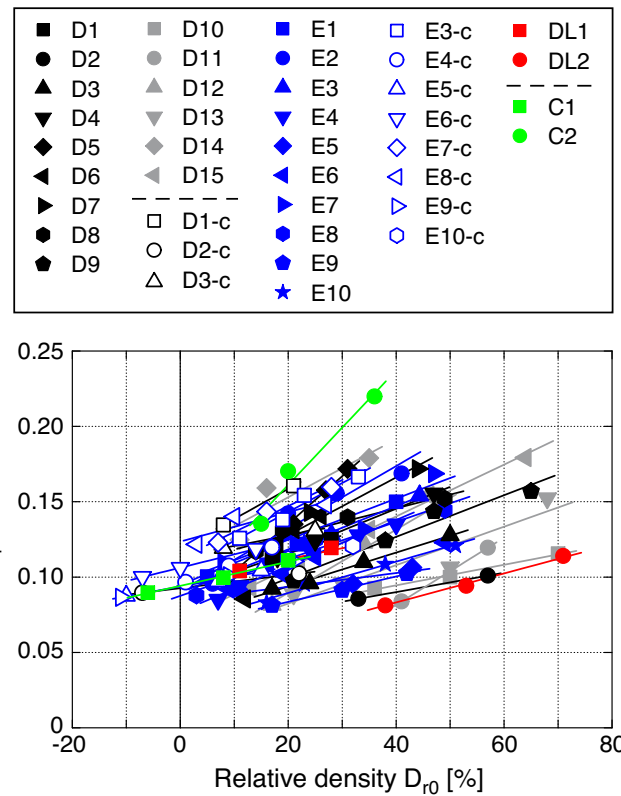
6 Influence of initial mean effective stress

The influence of initial mean effective stress p'_0 has been investigated on material D13. The samples were again prepared by the free fall method. For each of the four initial pressures $p'_0 = 50$, 100, 200 und 400 kPa, different relative densities and cyclic stress ratios have been tested. The effective stress paths measured for $p'_0 = 50$, 200 und 400 kPa and the same CSR value of 0.1 presented in Figure 16 resemble each other in shape. The only exception is a slightly larger inclination of the effective stress path during individual cycles in case of the lowest tested pressure. Furthermore, the sample under $p'_0 = 50$ kPa failed on the compression side, while failure took place during extension at higher pressures.

In Figure 17 the results of this test series are given in terms of CSR versus the number of cycles to failure. Based on these diagrams, the relationships between the liquefaction resistance $CRR(N_f = 10)$ and relative density D_{r0} presented in Figure 18 have been derived. Obviously, the inclination of the $CRR(N_f = 10)$-D_{r0} curves decreases with growing pressure. For low relative densities ($D_{r0} \approx$ 20 %) hardly any dependence of the liquefaction resistance on pressure can be concluded from Figure 18. At larger relative densities, the $CRR(N_f = 10)$ values clearly decrease with p'_0. Such reduction is in good accordance with the literature [2,5,28,38,39,42,54,70,81,85,98,100,107,125,127,147].

In order to analyze the pressure-dependence of the liquefaction resistance of medium dense to dense sand in more detail, the values $CRR(N_f = 10)$ for $D_{r0} = 50$ and 80 % and the four tested pressures have been read out of Figure 18. In Figure 19 the $CRR(N_f = 10)$ values for a given pressure p'_0 have been divided by the respective values for $p'_0 = $
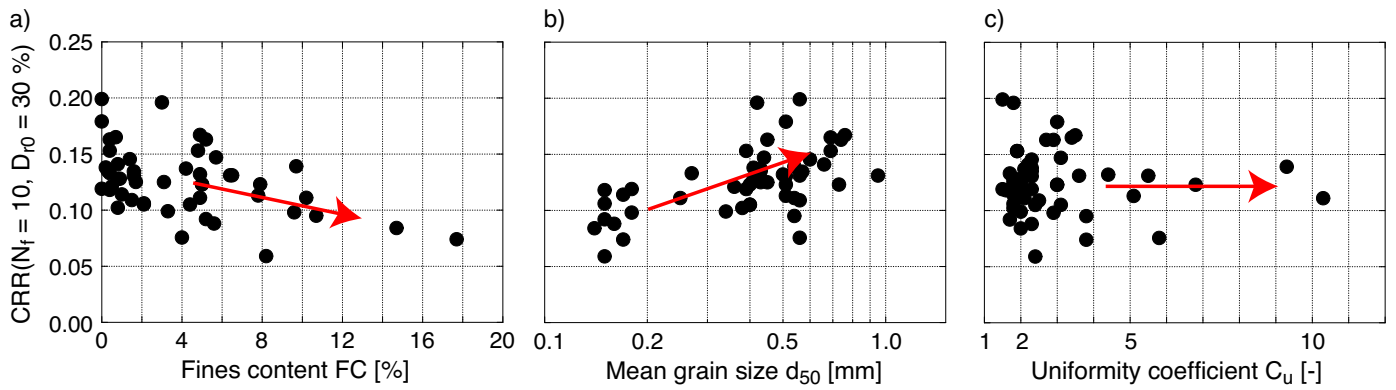
Fig. 15: *Liquefaction resistance $CRR(N_f = 10)$ at a relative density $D_{r0} = 30$ % as a function of the parameters of the grain size distribution curve, i.e. a) fines content FC, b) mean grain size d_{50} and c) uniformity coefficient C_u.*
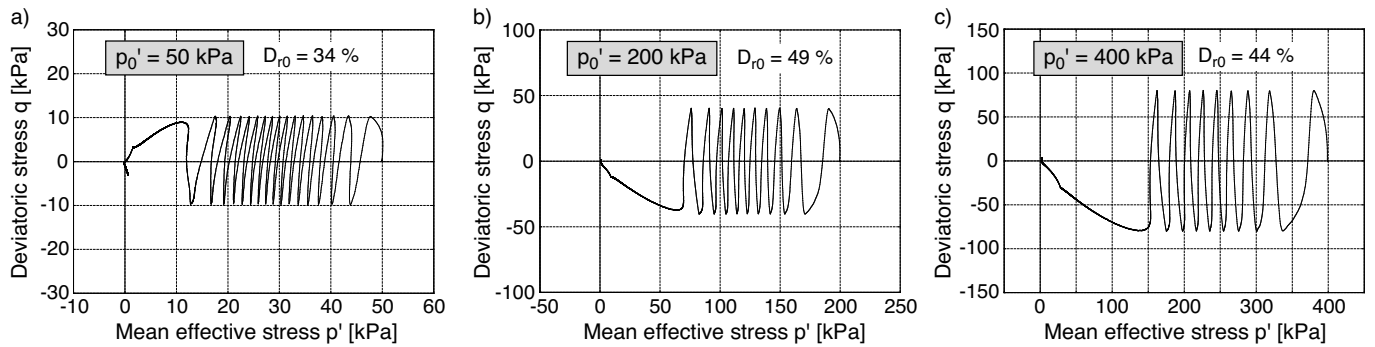
Fig. 16: *Effective stress paths from three tests with different initial mean effective stresses p_0' but identical cyclic stress ratio $CSR = q^{ampl}/(2p_0') = 0.1$: a) $p_0' = 50$ kPa, b) $p_0' = 200$ kPa, c) $p_0' = 400$ kPa*
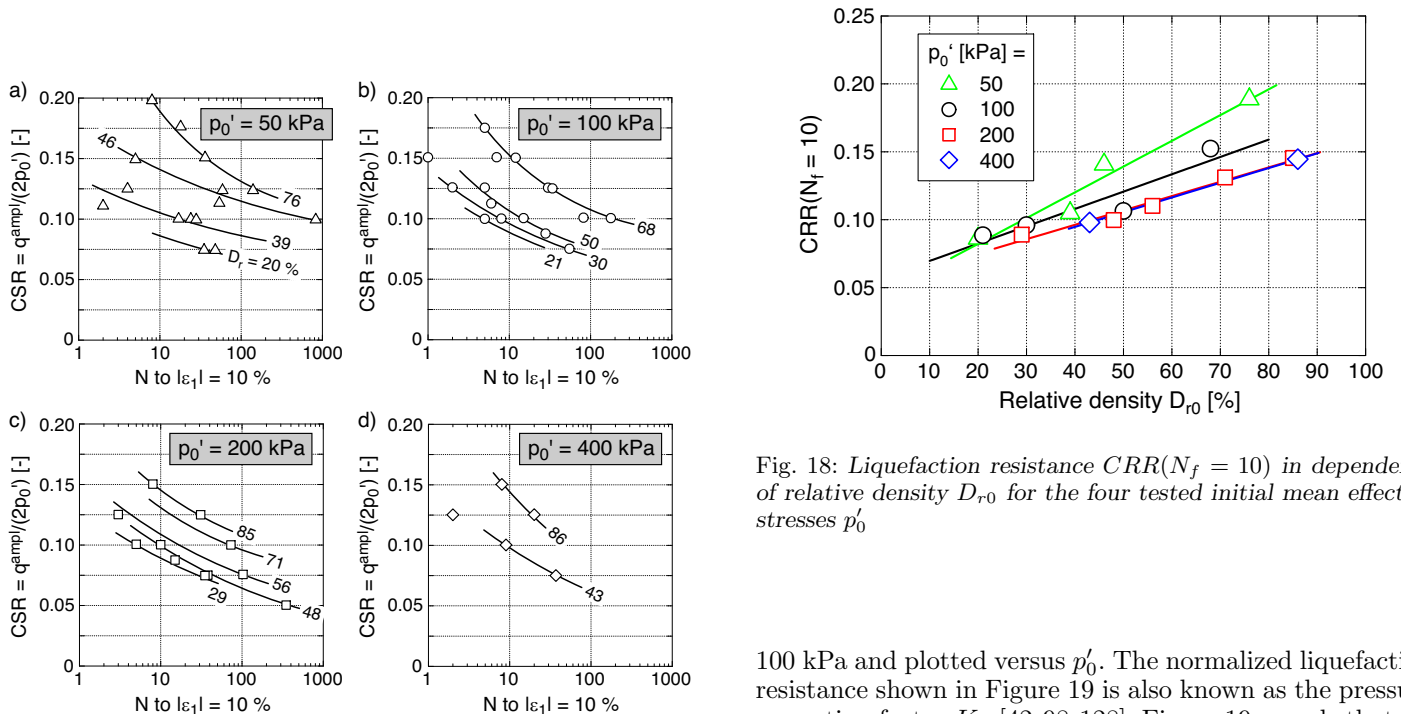
Fig. 17: *Cyclic stress ratio $CSR = q^{ampl}/(2p_0')$ as a function of the number of cycles to failure for the four tested initial mean effective stresses $p_0' = 50, 100, 200$ and 400 kPa*

Fig. 18: *Liquefaction resistance $CRR(N_f = 10)$ in dependence of relative density D_{r0} for the four tested initial mean effective stresses p_0'*

100 kPa and plotted versus p_0'. The normalized liquefaction resistance shown in Figure 19 is also known as the pressure correction factor K_σ [42,98,128]. Figure 19 reveals that for medium dense to dense sand the liquefaction resistance is about 20 % larger at low pressures ($p_0' = 50$ kPa) compared to the reference pressure $p_0' = 100$ kPa, while being about 15 % lower at higher pressures ($p_0' > 200$ kPa). The differences between K_σ at $p_0' = 200$ kPa and 400 kPa are negligible.
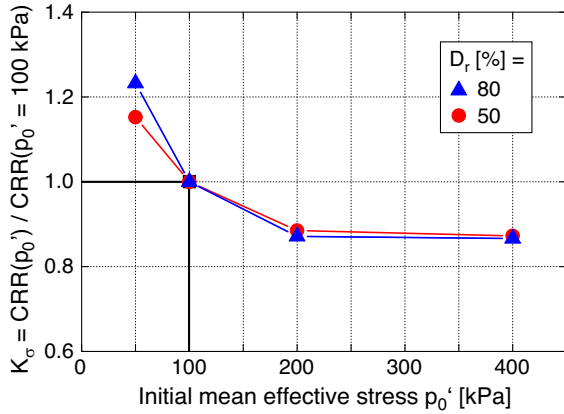
Fig. 19: *Pressure correction factor K_σ, defined as the liquefaction resistance $CRR(N_f = 10)$ at a given pressure p_0' divided by the respective value at $p_0' = 100$ kPa, in dependence of pressure p_0' for two different relative densities*

7   Influence of static shear stress

An element of soil in a slope is subjected to an initial static shear stress τ_0 superposing a K_0 stress state. The influence of the static shear stress on the liquefaction resistance depends on relative density, the initial mean effective stress and the chosen failure criterion, amongst others [11, 13, 39–42, 85, 91, 104, 120, 121, 126, 141, 142, 144]. The undrained cyclic strength can either increase or decrease due to the static shear stress. Therefore, the influence of static shear stress has to be experimentally investigated for the conditions of the site under consideration.

Such study has been performed by means of cyclic triaxial tests, where the initial static shear τ_0 is represented by an initial (or average) deviatoric stress $q_0 = q^{av} = 2\tau_0 > 0$. Samples of sand F8 have been prepared by the free fall method and tested at $p_0' = 100$ kPa and different values of q_0 (0, 15, 25, 40 and 50 kPa), corresponding to initial stress ratios of $\eta_0 = q_0/p_0' = 0$, 0.15, 0.25, 0.4 and 0.5. For each q_0 value, various initial densities and cyclic stress ratios have been tested. Schemes of the regions in the p'-q plane covered by the effective stress paths in this series are shown in Figure 20.

Typical results from tests with either $q^{ampl} > q^{av}$ or $q^{ampl} < q^{av}$ are provided in Figures 21 and 22, respectively. In the case $q^{ampl} > q^{av}$ the effective stress path exceeds the p' axis towards the extensional regime of the p'-q plane, while it keeps above the p' axis in the case $q^{ampl} < q^{av}$. In contrast to tests with isotropic consolidation (Figure 6), the samples cyclically loaded at higher q^{av} values do not fail by excessive strain amplitudes (i.e. an increase of axial strain on both the compressional and the extensional side, in particular at higher relative densities), but by an accumulation of strain finally reaching the failure criterion $|\varepsilon_1| = 10$ % (Figures 21a and 22a). The larger q^{av} the more pronounced is this accumulation and the less is the increase of the strain amplitude with increasing number of cycles. During the final phase of the test the effective stress path has the shape of an unsymmetric butterfly in case of $q^{ampl} > q^{av}$ (Figure 21c), while it is lens-shaped for $q^{ampl} < q^{av}$ (Figure 22c). While a state with zero effective stress is temporarily passed in the test with $q^{ampl} > q^{av}$, such full liquefaction is not reached in the case $q^{ampl} < q^{av}$ (except the post-test phase, when the axial strain is reduced to $\varepsilon_1 = 0$, Figure

22c).

The relationships between the cyclic stress ratio and the number of cycles to failure for all five tested q^{av} values (including the isotropic case) are collected in Figure 23. Figure 24 presents the same data in a single diagram, but restricted to relative densities 30 % $\le D_{r0} \le 39$ %. In that presentation, hardly any influence of q_0 can be detected. Based on the data in Figure 23 the $CRR(N_f = 10)$-D_{r0} diagram in Figure 25a has been established for the failure criterion $|\varepsilon_1| = 10$ %. Another diagram is provided for the lower strain $|\varepsilon_1| = 1$ % in Figure 25b. While different failure criteria (e.g. $|\varepsilon_1| = 1, 2, 5$ and 10 %) are reached in a single cycle in tests on loose sand with isotropic stresses, significant numbers of cycles can lie between these strains in case of tests with anisotropic consolidation, owed to the gradual accumulation of strain visible in Figures 21a and 22a. The differences between the five tested q^{av} values are small in Figure 25, but slightly more pronounced for the failure criterion defined by the lower axial strain. The variation of $CRR(N_f = 10)$ with q^{av} can be better judged from Figure 26. The presentation in that diagram restricts to a relative density $D_{r0} = 35$ % for which data for all tested q^{av} values are available. The curves in Figure 26 reveal a slight increase of the liquefaction resistance with increasing average deviatoric stress up to $q^{av} = 15$ kPa, respectively, and a subsequent moderate decrease, which is somewhat more pronounced for $|\varepsilon_1| = 1$ % than for $|\varepsilon_1| = 10$ %. An extension of this test series to larger q^{av} values is planned for the future.

8   Influence of partial saturation

During filling of the lake the deposited sands in the slopes will not get fully water-saturated. Some amount of air bubbles will remain in the pore spaces. Laboratory tests in which columns of various deposited soils were flooded by water lead to degrees of saturation between 75 and 95 %. Similar S_r values can be expected in the field. The partial saturated state may probably lead to an increased liquefaction resistance [33, 35, 78–80, 88, 101, 118, 119, 129, 136, 143, 145, 146]. This increase has been quantified as described in the following.

The tests were performed on samples of sand F2 prepared by the free fall method. First, several samples were tested fully water-saturated. Afterwards, samples with $S_r < 100$ % were prepared by omitting the CO_2 flushing as well as the water flushing under elevated pressure, and by using lower values of back pressure ($u_0 = 0$ to 200 kPa instead of the usual 500 kPa). The degree of saturation S_r was calculated based on the determined B value of Skempton [106], lying between 0.07 and 0.97 for the partially saturated samples. The conversion from B to S_r was undertaken by means of the following relationship after Biot [6, 7] and Bishop [8] (see also Yang [138, 139]):

$$B = \frac{\dfrac{1}{K_b} - \dfrac{1}{K_s}}{\dfrac{1}{K_b} - \dfrac{1+n}{K_s} + \dfrac{n}{K_w} + \dfrac{n(1-S_r)}{u_{abs}}} \qquad (1)$$

with the bulk modulus K_b of the grain skeleton, the bulk modulus K_s of the grains, the bulk modulus $K_w = 2.2$ GPa of water, porosity n and the absolute pore water pressure $u_{abs} = u + 98.1$ kPa. With the assumption of incompressible grains ($K_s \to \infty$) and after a reorganization with re-
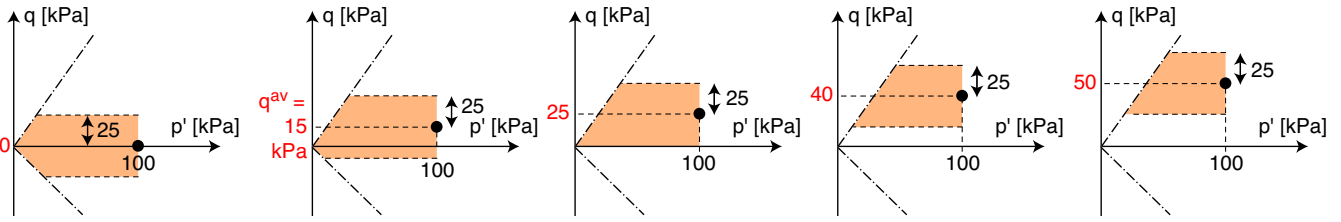
Fig. 20: *Regions in the p'-q plane covered by the effective stress paths in the series with different initial deviatoric stresses $q_0 = q^{av}$*
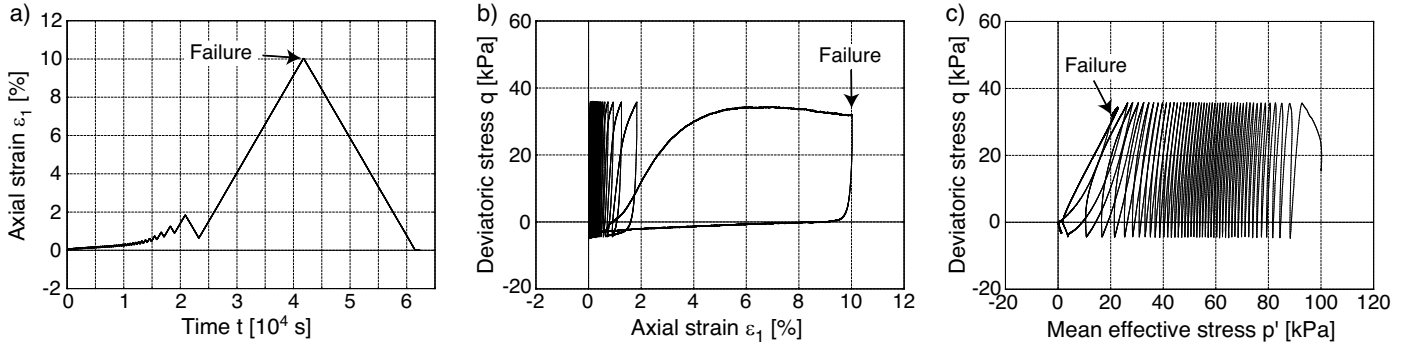
Fig. 21: *Results of a test with anisotropic initial stresses and $q^{ampl} > q^{av}$ ($q^{av} = 15$ kPa, $q^{ampl} = 20$ kPa, $D_{r0} = 37$ %)*
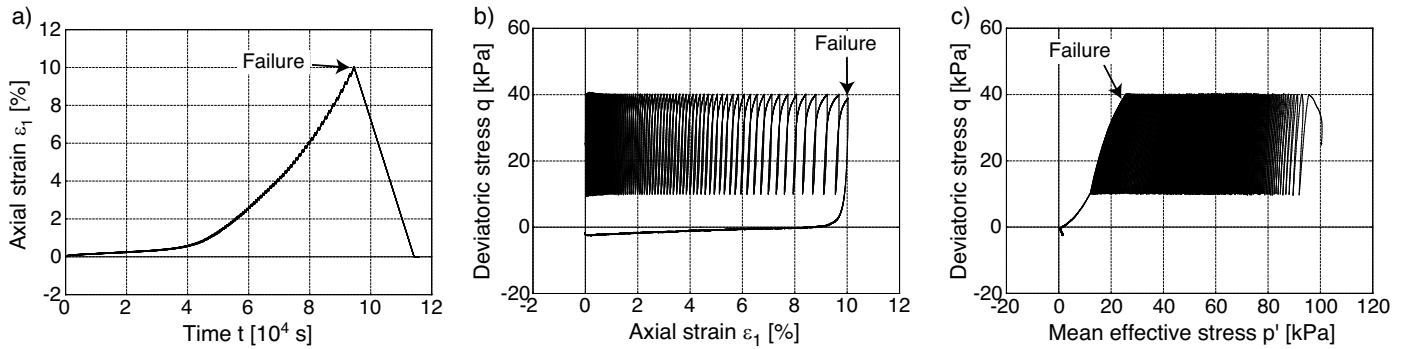
Fig. 22: *Results of a test with anisotropic initial stresses and $q^{ampl} < q^{av}$ ($q^{av} = 25$ kPa, $q^{ampl} = 15$ kPa, $D_{r0} = 40$ %)*

spect to S_r the formula reads:

$$S_r = 1 - \frac{1 - B\left(1 + n\frac{K_b}{K_w}\right)}{Bn\frac{K_b}{u_{abs}}} \tag{2}$$

While B, n and u_{abs} are known for each sample, the bulk modulus of the grain skeleton has been calculated in dependence of effective mean stress p' from the relationship $K_b = 60.0(p'/p_{atm})^{0.78}p_{atm}$ derived from the data of oedometric compression tests ($p_{atm} = 100$ kPa). According to Eq. (2) the B values of 0.07 to 0.97 correspond to degrees of saturation S_r lying between 49 und 99 %.

Effective stress paths from tests with nearly full saturation ($S_r = 99.4$ %) and partial saturation ($S_r = 62.6$ %) are compared in Figure 27. Although a larger stress amplitude has been chosen for the test on the partially saturated sample, the necessary number of cycles till failure of this sample was much larger than for its nearly water-saturated counterpart. Furthermore, the inclination of the effective stress path measured for the partially saturated sample resembles that in a drained test (inclination 3:1 in the q-p'

diagram), owed to the comparably large compressibility of the pore fluid containing air bubbles.

The CSR-N diagram in Figure 28 reveals a strong increase of the liquefaction resistance with decreasing degree of saturation. The liquefaction resistance $CRR(N_f = 10)$ grows by about 40 % if S_r drops from 100 % to 88 %.

In the field the degree of saturation and its impact on the liquefaction resistance could be quantified by means of measurements of the P wave velocity as outlined in [138–140].

9 Influence of a monotonic preloading

The effect of a monotonic preloading on the liquefaction resistance has seldomly been studied in the literature. In a few publications a decrease of the susceptibility to liquefaction due to overconsolidation was reported [45, 48, 110]. The strong alteration of the sand response to undrained monotonic loading caused by a drained monotonic preloading has been demonstrated in [10, 17–20, 26, 30], however. A monotonic loading by a temporal fill could be a possible measure to increase the liquefaction resistance of deposited soils in the dumps.
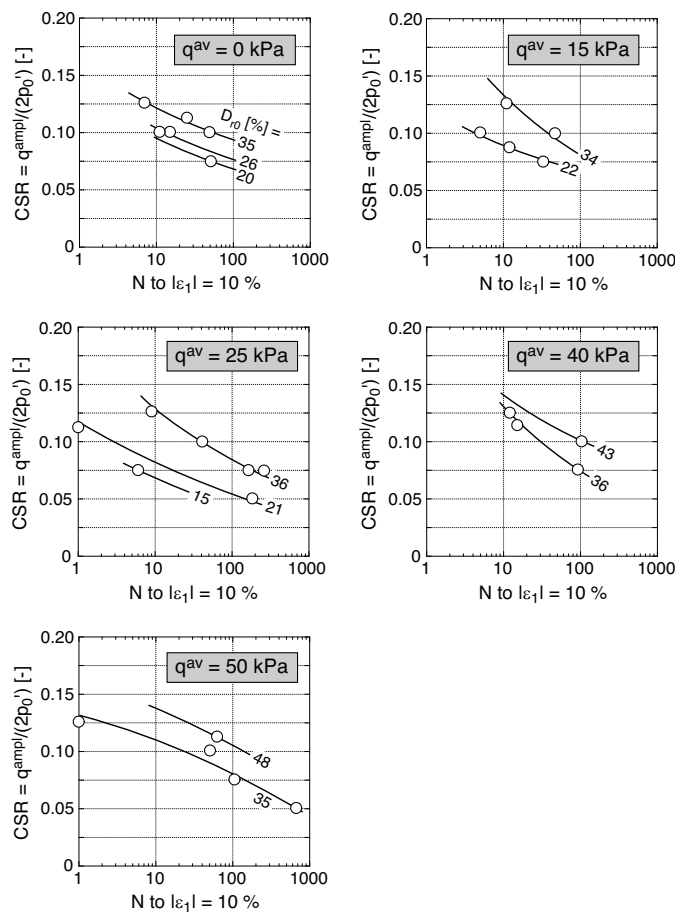
Fig. 23: *Cyclic stress ratio $CSR = q^{ampl}/(2p'_0)$ as a function of the number of cycles to failure ($|\varepsilon_1| = 10$ %) for the five tested average deviatoric stresses $0 \leq q^{av} \leq 50$ kPa*
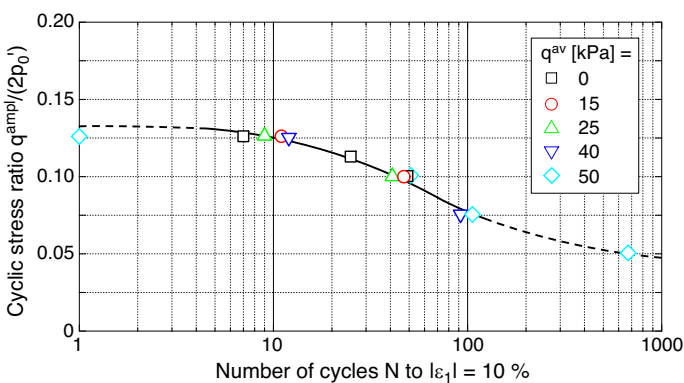
Fig. 24: *Cyclic stress ratio $CSR = q^{ampl}/(2p'_0)$ as a function of the number of cycles to failure ($|\varepsilon_1| = 10$ %) for the five tested average deviatoric stresses $0 \leq q^{av} \leq 50$ kPa and similar relative densities in the range 30 % $\leq D_{r0} \leq 39$ %*
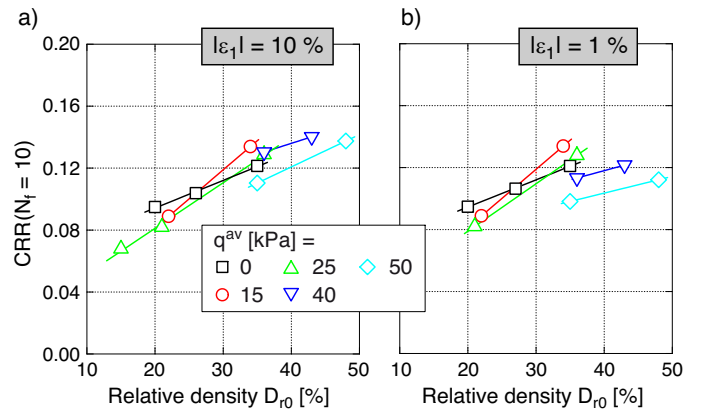
Fig. 25: *Cyclic stress ratio causing failure defined as either a) $|\varepsilon_1| = 10$ % or b) $|\varepsilon_1| = 1$ % in $N_f = 10$ cycles as a function of relative density D_{r0}*
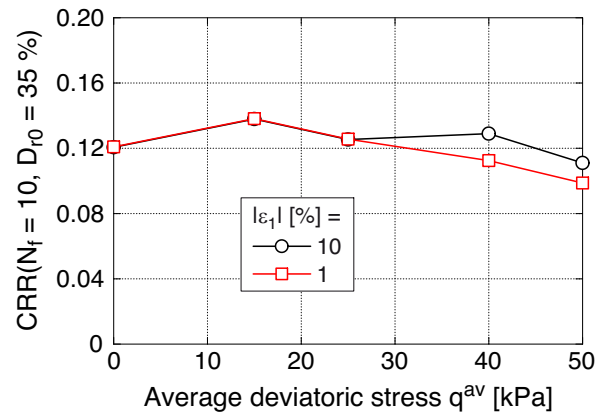
Fig. 26: *Cyclic stress ratio causing failure defined as either $|\varepsilon_1| = 10$ % or $|\varepsilon_1| = 1$ % in $N_f = 10$ cycles for samples with a relative density of $D_{r0} = 35$ % as a function of average deviatoric stress q^{av}*
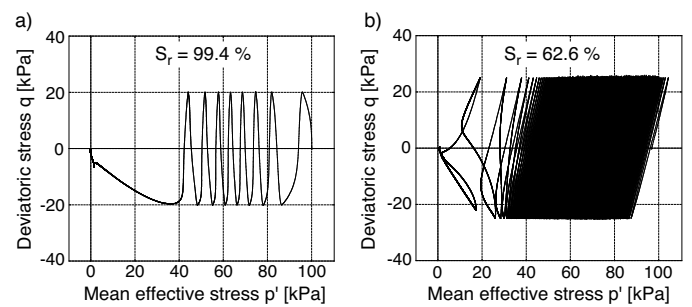
Fig. 27: *Effective stress paths measured in tests with a) nearly full saturation ($S_r = 99.4$ %) and b) partial saturation ($S_r = 62.6$ %)*
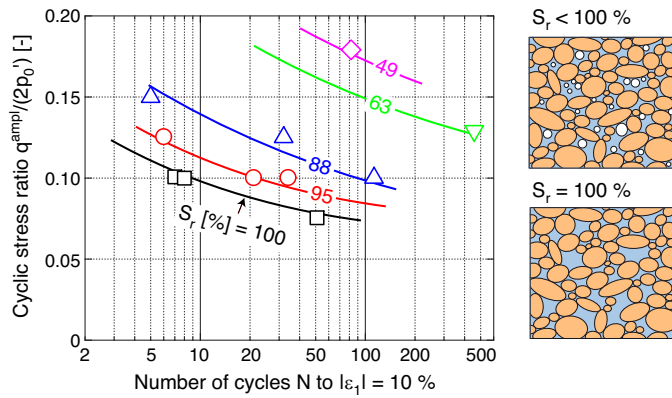
Fig. 28: *Cyclic stress ratio $CSR = q^{ampl}/(2p_0')$ as a function of the number of cycles to failure ($|\varepsilon_1| = 10$ %) for samples with different degrees of saturation S_r and relative densities in the range 24 % $\leq D_{r0} \leq$ 39 %.*

In order to quantify the effect, tests with a drained monotonic preloading have been performed on sand F8. Again, the samples were prepared by the free fall method. Both an isotropic and a deviatoric preloading have been tested. In case of the isotropic preloading (see scheme in Figure 30) the mean effective stress has been increased to $p' = 120$ kPa or 150 kPa, followed by an unloading to $p_0' = 100$ kPa. In case of the deviatoric preloading (see scheme in Figure 31), starting from $p_0' = 100$ kPa the axial stress was increased by $\Delta\sigma_1 = \Delta q = 20$ kPa or 50 kPa, respectively, followed by an unloading to the isotropic stress conditions. For both the isotropic and the deviatoric preloading, the compaction of the samples during the preloading phase was rather small, corresponding to changes of the relative density of $\Delta D_{r0} = 2$ % at maximum. After the drained preloading the drainage was closed and the cyclic loading was started.

Effective stress paths for a non-preloaded sample and two samples subjected to either an isotropic preloading with $\Delta p' = 50$ kPa or a deviatoric preloading with $\Delta q = 50$ kPa are compared in Figure 29. Despite similar relative densities at the start of the undrained cyclic loading phase, the preloaded samples needed a larger number of cycles to failure and showed some tendencies to a cylic mobility during the final phase of the tests.

The increase of the liquefaction resistance with increasing magnitude of monotonic preloading ($\Delta p'$ or Δq) becomes also clear from the CSR-N diagrams in Figures 30 and 31 and from the $CRR(N_f = 10)$-D_{r0} graph in Figure 32. The liquefaction resistance for a relative density of 30 % is further analyzed in Figure 33, where the $CRR(N_f = 10)$ for the preloaded samples are referred to the corresponding value of their non-preloaded counterparts and plotted versus $\Delta p'$ or Δq, respectively. According to this diagram, an isotropic preloading with $\Delta p' = 50$ kPa and a deviatoric preloading with $\Delta q = 50$ kPa cause both an increase of the liquefaction resistance by about 40 %. At smaller magnitudes of preloading ($\Delta p'$ or $\Delta q = 20$ kPa) the deviatoric preloading is slightly more effective than the isotropic one. Since the liquefaction resistance at equal density and stress depends on the preloading, the preloading seems to change the fabric of the sand, rendering it more resistant to the subsequent undrained cyclic loading.

10 Influence of a vibrational preloading

In the dumps of the lignite opencast mines a vibrational preloading of the deposited soils is caused by general mining operations (amongst others by the powerful spreaders, Figure 1) or by smaller earthquakes which irregularly occur. An increase of the liquefaction resistance of sand by a vibrational preloading with moderate amplitudes has been demonstrated by numerous researchers [3, 9, 24, 27, 44, 46, 64, 76, 83, 96, 99, 108, 113, 122, 132]. It is again caused by subtle changes in the sand microstructure. In the previous studies, however, the vibrational preloading was applied on either dry or fully water-saturated sand. It was unclear so far if a similar effect is observed in case that the vibrational preloading is applied to moist sand, where particle re-orientations are hindered by capillary effects at the grain contacts.

The effect of a vibrational preloading applied on moist deposited sand has been studied in triaxial tests on sand D8. Samples were prepared by the free fall method and subsequently vibrated by means of a shaking table. The shaking table generates both a horizontal and a vertical vibration simultaneously, where the amplitude of the vertical displacement (u_v^{ampl}) is slightly smaller than that in the horizontal (u_h^{ampl}) direction. Two different amplitudes (amplitude 1: $u_{h1}^{ampl} = 0.3$ mm, $u_{v1}^{ampl} = 0.2$ mm; amplitude 2: $u_{h2}^{ampl} = 0.6$ mm, $u_{v2}^{ampl} = 0.4$ mm) have been applied with two different durations (2 and 10 min). Considering the operational frequency of the shaking table of 50 Hz, these durations lead to the application of 6000 or 30000 cycles, respectively. These high numbers of cycles are representative for the preloading caused by general mining operations. The amplitudes applied in this test series were, however, larger than those usually occuring in the dumps. After this vibrational preloading the samples were built into the triaxial device, water-saturated and tested under an undrained cyclic loading with different amplitudes started from $p_0' = 100$ kPa.

Effective stress paths for samples subject to a different vibrational preloading history are collected in Figure 34. With growing intensity of the preloading, i.e. with increasing number of cycles and/or amplitude during that phase, the number of cycles to failure and the tendency to a cyclic mobility during the subsequent undrained cyclic loading increases, despite similar relative density. The CSR-N and $CRR(N_f = 10)$-D_{r0} diagrams in Figures 35 and 36 confirm the increase of the liquefaction resistance with increasing intensity of the vibrational preloading for a given relative density. Therefore, such preloading has a positive effect regarding the liquefaction resistance even if it is applied on moist soil.

11 Influence of membrane penetration

Results of undrained cyclic triaxial tests on sand can be falsified by membrane penetration effects [4, 14, 29, 34, 52, 56, 57, 62, 65–67, 67, 69, 73–75, 77, 89, 90, 105, 114–116, 124]. The accumulation of pore water pressure is delayed by these effects, leading to an overestimation of the liquefaction resistance. The effect of membrane penetration increases with increasing grain size [75]. A possible method to quantify these effects is the testing of samples with different ratios of membrane area A_M and sample volume V. The effects are more pronounced for higher values of A_M/V.
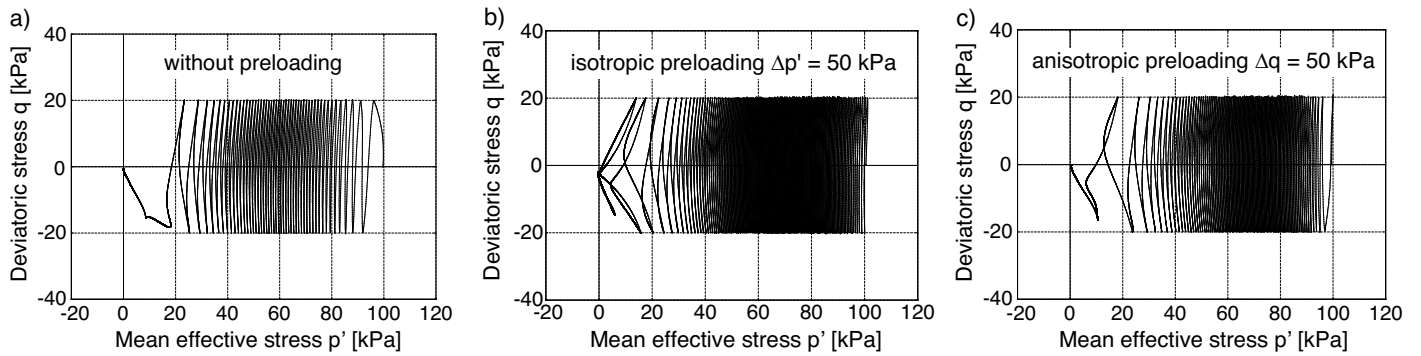
Fig. 29: Effective stress paths from tests with a different monotonic preloading: a) no preloading, b) drained isotropic preloading with $\Delta p' = 50$ kPa, c) drained deviatoric preloading with $\Delta q = 50$ kPa. All tests with relative densities in the range $32\ \% \leq D_{r0} \leq 38\ \%$.
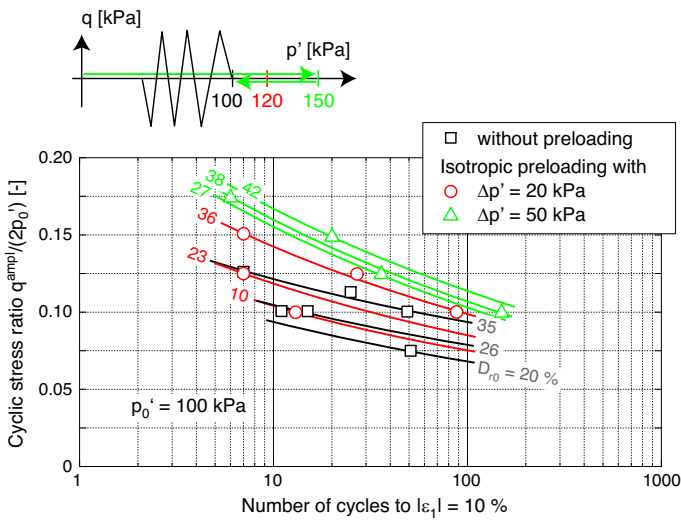
Fig. 30: *Cyclic stress ratio $CSR = q^{\mathrm{ampl}}/(2p_0')$ as a function of the number of cycles to failure ($|\varepsilon_1| = 10\ \%$): Influence of a drained monotonic preloading along an isotropic stress path*
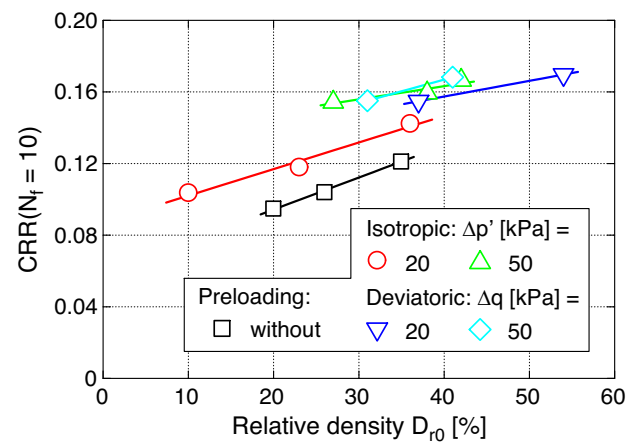
Fig. 32: *Liquefaction resistance $CRR(N_f = 10)$ in dependence of relative density D_{r0} for different types and magnitudes of drained monotonic preloading*
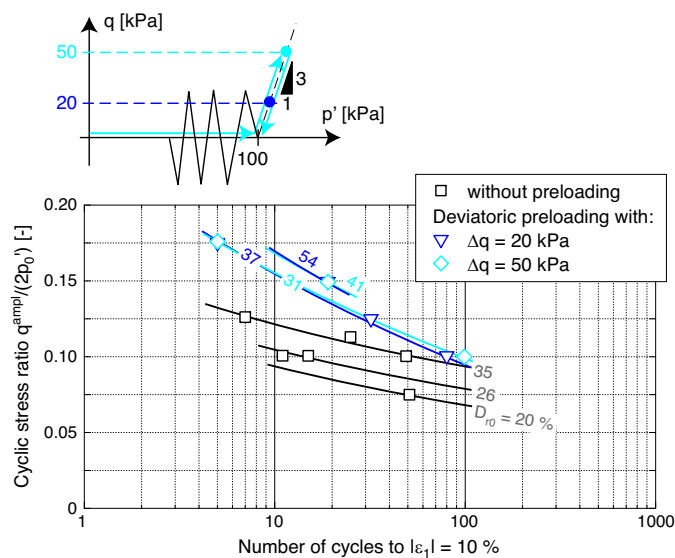
Fig. 31: *Cyclic stress ratio $CSR = q^{\mathrm{ampl}}/(2p_0')$ as a function of the number of cycles to failure ($|\varepsilon_1| = 10\ \%$): Influence of a drained monotonic preloading along a deviatoric stress path*
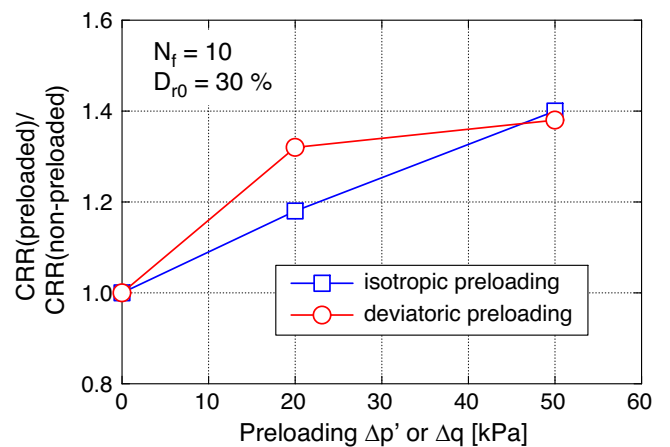
Fig. 33: *Increase of the liquefaction resistance $CRR(N_f = 10)$ in dependence of the magnitude $\Delta p'$ or Δq of drained monotonic preloading*
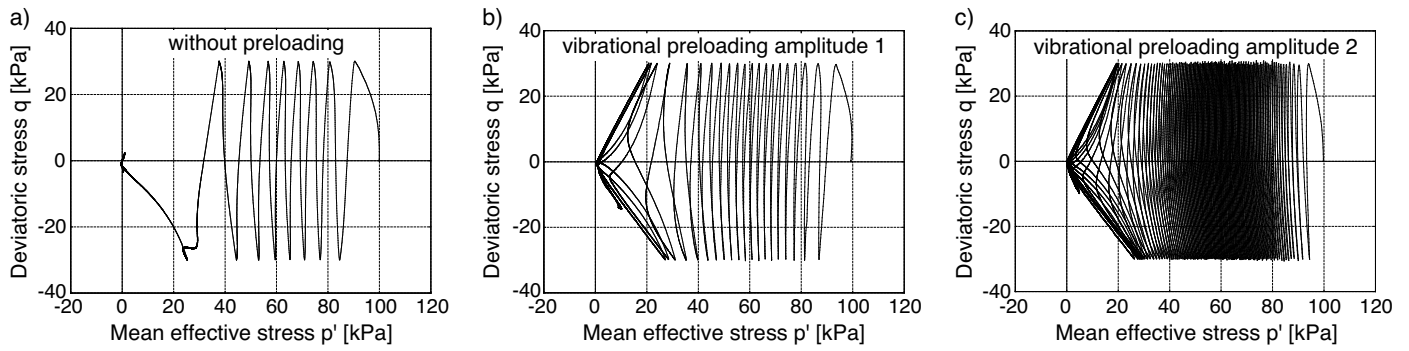
Fig. 34: Effective stress paths from tests on samples with different intensities of vibrational preloading but equal stress amplitude $q^{\text{ampl}} = 30$ kPa: a) without preloading ($D_{r0} = 37$ %), b) 2 min vibration (6000 cycles) with amplitude 1 ($u_{h1}^{\text{ampl}} = 0.3$ mm, $u_{v1}^{\text{ampl}} = 0.2$ mm, $D_{r0} = 47$ %), c) 2 min vibration with amplitude 2 ($u_{h2}^{\text{ampl}} = 0.6$ mm, $u_{v2}^{\text{ampl}} = 0.4$ mm, $D_{r0} = 46$ %)
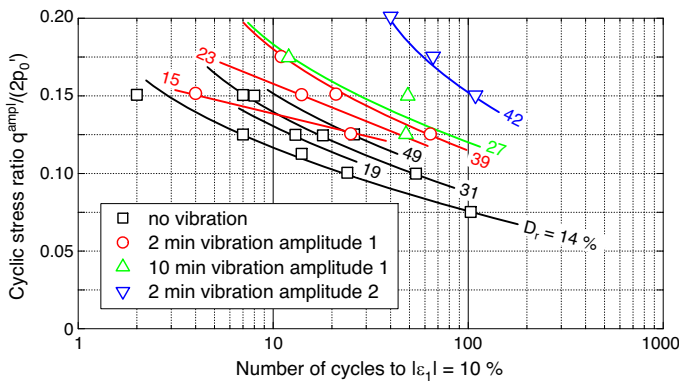
Fig. 35: *Cyclic stress ratio $CSR = q^{\text{ampl}}/(2p_0')$ as a function of the number of cycles to failure ($|\varepsilon_1| = 10$ %): Influence of a vibrational preloading*
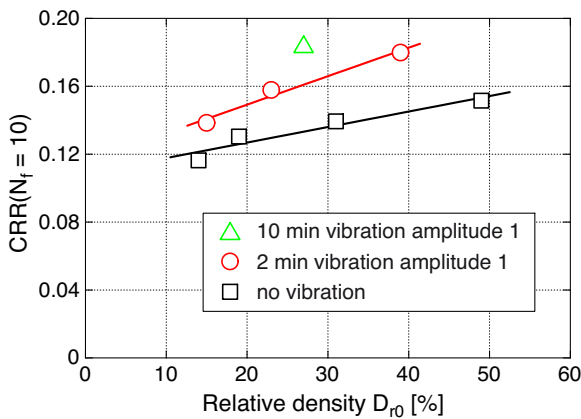
Fig. 36: *Liquefaction resistance $CRR(N_f = 10)$ in dependence of relative density D_{r0} for different intensities of vibrational preloading*

In case of the deposited soils the fines content could help reducing the membrane penetration effects. With the aim of quantification a series of undrained cyclic triaxial tests was performed on sand F8 ($d_{50} = 0.56$ mm, $FC = 1.5$ %). Beside the standard sample geometry ($d = h = 100$ mm, $A_M/V = 0.4$), smaller ($d = h = 50$ mm, $A_M/V = 0.8$) and larger ($d = h = 150$ mm, $A_M/V = 0.3$) samples were tested. The three different sample sizes are shown on the photos in Figure 37. According to the A_M/V ratios, membrane

penetration effects should be twice larger for the smallest tested geometry compared to the standard samples. They should further decrease if the largest geometry is compared to the standard one.

Fig. 37: Samples with different sizes: $d = h = 50$ mm (left), $d = h = 100$ mm (middle), $d = h = 150$ mm (right)

Effective stress paths measured for the three different sample sizes in tests with similar initial densities and same loading conditions are given in Figure 38. With the exception of the slightly larger inclination of the stress path in case of the smallest tested sample size (which is sometimes regarded as a sign for membrane penetration) and failure occurring on either the extensional ($d = h = 50$ mm and 150 mm) or the compressional side ($d = h = 100$ mm), the shape of the paths is quite similar. Figure 39 presents the liquefaction resistance $CRR(N_f = 10)$ as a function of relative density D_{r0} for the different sample sizes. Hardly any influence of the sample size can be concluded from this diagram. Therefore, membrane penetration effects seem to be small for the tested deposited soils, probably due to their fines content reducing the roughness of the contact surface between sample and membrane.

12 Cyclic loading with constant strain amplitude

For an evaluation of the liquefaction risk by means of the cyclic strain approach of Dobry et al. [21] tests with constant strain amplitudes are necessary. Several such tests have been performed on sand F8 using axial strain amplitudes in the range $2 \cdot 10^{-4} \leq \varepsilon_1^{\text{ampl}} \leq 2 \cdot 10^{-3}$. The undrained cyclic loading was started at $p_0' = 100$ kPa. A typical effective stress path from a test with $D_{r0} = 38$ % and $\varepsilon_1^{\text{ampl}} = 10^{-3}$ is shown in Figure 40a. In accordance with earlier studies [49, 50, 93, 134] it has the shape of a
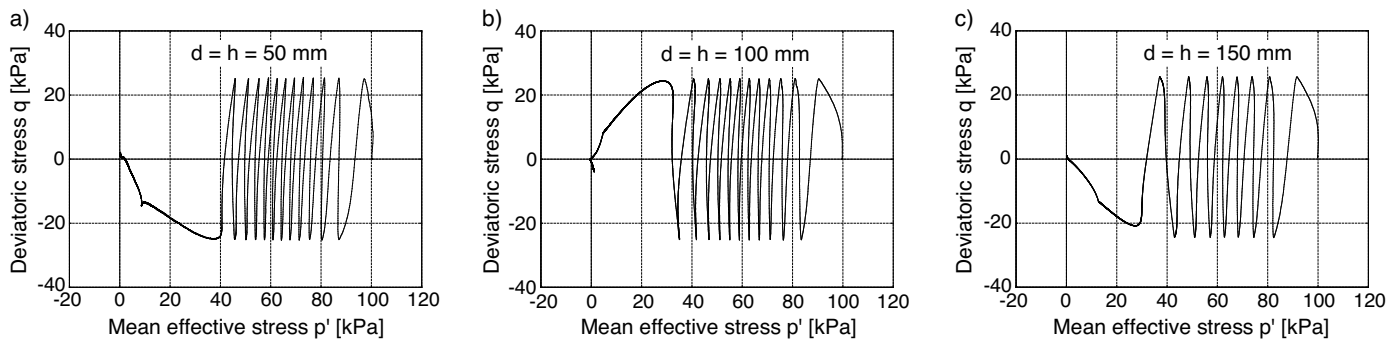
Fig. 38: Effective stress paths from tests on samples with different sizes: a) $d = h = 50$ mm ($D_{r0} = 35$ %), b) $d = h = 100$ mm ($D_{r0} = 31$ %), c) $d = h = 150$ mm ($D_{r0} = 26$ %)
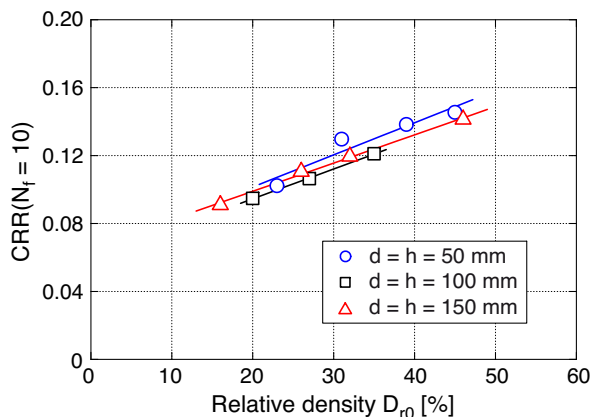
Fig. 39: *Liquefaction resistance $CRR(N_f = 10)$ in dependence of relative density D_{r0} for different sample sizes*

horizontal fir tree. Figure 40b collects the curves of the pore water pressure ratio $r_u = u^{\mathrm{acc}}/p_0'$ versus the number of cycles for the various tested strain amplitudes. In some cases tests with the same amplitude have been performed twice, partially in two different test devices, to prove repeatability. The results from these pairs of tests agree well. The data in Figure 40b show the expected increase of the rate of pore water pressure accumulation with increasing strain amplitude. Based on the test data diagrams as that shown in Figure 40c were derived as proposed by Dobry et al. [21]. This representation allows the estimation of the accumulated pore water pressure ratio r_u in dependence of shear strain amplitude $\gamma^{\mathrm{ampl}} = 1.5\varepsilon_1^{\mathrm{ampl}}$ for different numbers of cycles and a certain relative density ($D_{r0} = 26$ % in case of Figure 40c).

13   Summary and conclusions

A parametric study on the liquefaction resistance of deposited sands in dumps of lignite opencast mines has been performed using undrained cyclic triaxial tests. Undisturbed samples have been taken on a dump site by ground freezing. From the same material also disturbed samples have been reconstituted by different methods. From a comparison of these different types of samples it can be concluded that a sample preparation method, where moist sand falls from a certain height into the split mould, is suitable for reproducing the depositional process in the dumps, leading to a similar initial fabric. This method has thus

been used for all further parametric studies.

From tests on more than 50 different sands, mainly originating from the dumps or the excavation sites of the opencast mines, a large influence of the grain size distribution curve on the liquefaction resistance could be concluded. At constant relative density the undrained cyclic strength tends to decrease with increasing fines content (although the fines are plastic) and to increase with the mean grain size. No clear trend can be found in the data with respect to a possible influence of the uniformity coefficient.

The influence of initial mean effective stress was found small for low relative densities, while the liquefaction resistance decreased with p_0' for medium dense to dense sand. The influence of an average deviatoric shear stress on the number of cycles to failure was found rather small in the range of tested values $0 \leq q^{\mathrm{av}} \leq 50$ kPa, while p_0' was 100 kPa. A small increase of the liquefaction resistance up to $q^{\mathrm{av}} = 15$ kPa was followed by a moderate reduction at larger q^{av} values.

Furthermore, an increase of the undrained cyclic strength with decreasing degree of saturation and due to a drained monotonic preloading along isotropic or deviatoric paths was demonstrated. A vibrational preloading has a similar positive effect, despite its application in the moist state, where particle reorientations are hindered by capillary effects. From a comparison of samples with different sizes it could be concluded that membrane penetration effects are negligible for the tested deposited materials.

For an evaluation of the liquefaction risk by means of the cyclic strain approach of Dobry et al. [21] tests with constant strain amplitudes have been performed. Diagrams giving the accumulated pore pressure as a function of shear strain amplitude and number of cycles were developed based on these tests.

The results of the undrained cyclic triaxial tests presented in this paper will be further used for the proof against liquefaction for the dumps of the opencast mines, either by means of correlations with CPT tip resistance or shear wave velocity [?], or by numerical simulations. In the latter case the material constants of the applied constitutive models are calibrated based on the test data [131].

References

[1] L. Ahorner. Abschätzung der statistischen Wiederkehrperiode von starken Erdbeben im Gebiet von Köln auf Grund von geologisch-tektonischen Beobachtungen an aktiven Störungen. In *Mitteilungen der Deutschen Geophysikalischen Gesellschaft*, volume 2, pages 2–9, 2001.
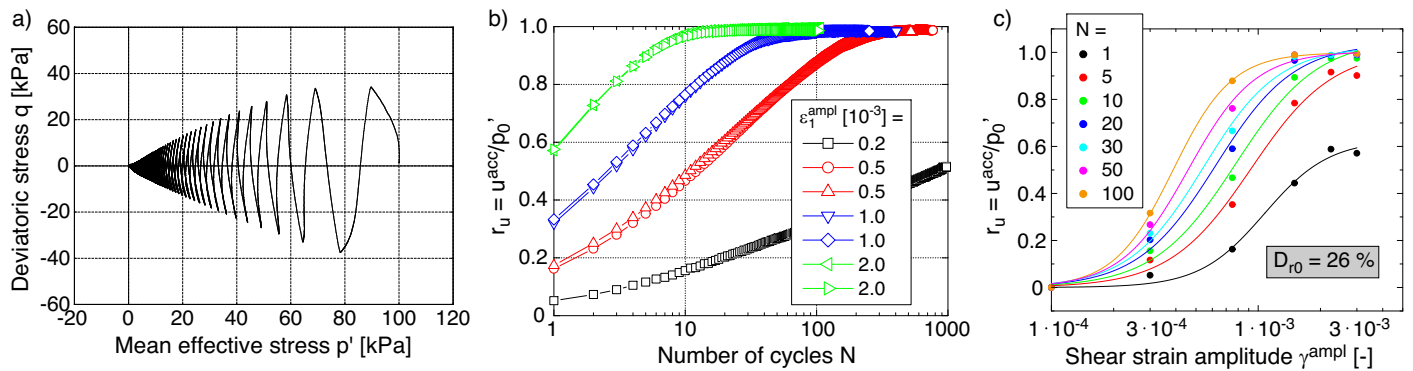
Fig. 40: Results of undrained cyclic triaxial tests with constant strain amplitudes ε_1^{ampl}: a) Typical effective stress path from a test with $D_{r0} = 38\,\%$ and $\varepsilon_1^{ampl} = 10^{-3}$, b) Increase of accumulated pore water pressure ratio $r_u = u^{acc}/p_0'$ with increasing number of cycles in tests with different strain amplitudes ε_1^{ampl} and similar initial relative densities ($30\,\% \le D_{r0} \le 44\,\%$), c) Accumulated pore water pressure ratio r_u as a function of shear strain amplitude $\gamma^{ampl} = 1.5\varepsilon_1^{ampl}$ for different numbers of cycles and a relative density of $D_{r0} = 26\,\%$

[2] F. Amini and Z. Qi. Liquefaction testing on stratified silty sands. *Journal of Geotechnical and Geoenvironmental Engineering, ASCE*, 126(3):208–217, 2000.

[3] K.H. Andersen. Bearing capacity under cyclic loading - offshore, along the coast, and on land. The 21st Bjerrum Lecture presented in Oslo, 23 November 2007. *Canadian Geotechnical Journal*, 46(5):513–535, 2009.

[4] G. Baldi and R. Nova. Membrane penetration effects in triaxial testing. *Journal of Geotechnical Engineering, ASCE*, 110(3):403–420, 1984.

[5] M. H. Baziar and H. Sharafi. Assessment of silty sand liquefaction potential using hollow torsional tests - An energy approach. *Soil Dynamics and Earthquake Engineering*, 31(3):857–865, 2011.

[6] M. A. Biot. Theory of propagation of elastic waves in a fluid saturated porous solid. *J. Acoust. Soc. Am.*, 28:168–191, 1956.

[7] M. A. Biot. Mechanics of deformation and acoustic propagation in porous media. *J. Appl. Phys.*, 33:1482–1498, 1962.

[8] A. W. Bishop. The influence of an undrained change in stress on the pore pressure in porous media of low compressibility. *Géotechnique*, 23(3):435–442, 1973.

[9] L. Bjerrum. Geotechnical problems involved in foundations of structures in the North Sea. *Géotechnique*, 23(3):319–358, 1973.

[10] D.C. Bobei, D. Wanatowski, M.M. Rahman, S.R. Lo, and C.T. Gnanendran. The effect of drained pre-shearing on the undrained behaviour of loose sand with a small amount of fines. *Acta Geotechnica*, 8(3):311–322, 2013.

[11] R. W. Boulanger. Relating Kα to relative state parameter index. *Journal of Geotechnical and Geoenvironmental Engineering, ASCE*, 129(8):770–773, 2003.

[12] T. Camelbeeck, T. vanEck, R. Pelzing, L. Ahorner, L. Loohuis, H.W. Haak, P. Hoang-Trong, and D. Hollnack. The 1992 Roermond earthquake, the Netherlands, and its aftershocks. *Geologie en Mijnbouw*, 73:181–197, 1994.

[13] G. Castro and S.J. Poulos. Factors affecting liquefaction and cyclic mobility. *Journal of the Geotechnical Engineering Division, ASCE*, 103(GT6):501–516, 1977.

[14] J.W. Choi and I. Ishibashi. An experimental method for determining membrane penetration. *Geotechnical Testing Journal, ASTM*, 15(4):413–417, 1992.

[15] M. Derakhshandi, E. M. Rathje, K. Hazirbaba, and S. M. Mirhosseini. The effect of plastic fines on the pore pressure generation characteristics of saturated sands. *Soil Dynamics and Earthquake Engineering*, 28:376–386, 2008.

[16] E. Dermietzel. Zur Frage der Anfangsstandfestigkeit von Absetzerschüttungen im tiefen Tagebau. *Braunkohle*, (11):406–412, 1970.

[17] T. Doanh, Ph. Dubujet, and X. Protière. On the undrained strain-induced anisotropy of loose sand. *Acta Geotechnica*, 8(3):293–309, 2013.

[18] T. Doanh, Ph. Dubujet, and G. Touron. Exploring the undrained induced anisotropy of Hostun RF loose sand. *Acta Geotechnica*, 5(4):239–256, 2010.

[19] T. Doanh, Z. Finge, and S. Boucq. Effects of previous deviatoric strain histories on the undrained behaviour of Hostun RF loose sand. *Geotechnical and Geological Engineering*, 30(4):697–712, 2012.

[20] T. Doanh, Z. Finge, S. Boucq, and Ph. Dubujet. Histotropy of Hostun RF loose sand. In W. Wu and H.-S. Yu, editors, *Modern Trends in Geomechanics*, volume 106, pages 399–411. Springer, 2006.

[21] R. Dobry, R.S. Ladd, F.Y. Yokel, R.M. Chung, and D. Powell. Prediction of pore pressure buildup and liquefaction of sands during earthquakes by the cyclic strain method. Technical Report 138, U.S. Department of Commerce, National bureau of standards, 1982. NBS Building science series.

[22] C. Drebenstedt. Bedeutung des Kippenmodells für geomechanische Prognosen - Einfluss der Tagebautechnologie. Vortrag Geotechnisches Symposium - Standsicherheit von Kippen des Braunkohlenbergbaus, 2013.

[23] J.-C. Dupla and J. Canou. Cyclic pressuremeter loading and liquefaction properties of sands. *Soils and Foundations*, 43(2):17–31, 2003.

[24] J.J. Emery, W.D.L. Finn, and K.W. Lee. Uniformity of saturated sand specimen. Technical Report STP523, pp. 182-194, ASTM, 1973.

[25] M.D. Evans and S. Zhou. Liquefaction behavior of sand-gravel composites. *Journal of Geotechnical Engineering, ASCE*, 121(3):287–298, 1995.

[26] Z. Finge, T. Doanh, and P. Dubujet. Undrained anisotropy of Hostun RF loose sand: new experimental investigations. *Canadian Geotechnical Journal*, 43:1195–1212, 2006.

[27] W.D.L. Finn, P.L. Bransby, and D.J. Pickering. Effect of strain history on liquefaction of sand. *Journal of the Soil Mechanics and Foundations Division, ASCE*, 96(SM6):1917–1934, 1970.

[28] S. Frydman, D. Hendron, H. Horn, J. Steinbach, R. Baker, and B. Shaal. Liquefaction study of cemented sand. *Journal of the Geotechnical Engineering Division, ASCE*, 106(GT3):275–297, 1980.

[29] S. Frydman, J.G. Zeitlen, and I. Alpan. The membrane effect in triaxial testing on granular soils. *Journal of Testing and Evaluation*, 1(1):37–41, 1973.

[30] A. Gajo and L. Piffer. The effects of preloading history on the undrained behaviour of saturated loose sand. *Soils and Foundations*, 39(6):43–54, 1999.

[31] V.N. Ghionna and D. Porcino. Liquefaction resistance of undisturbed and reconstituted samples of a natural coarse sand from undrained triaxial tests. *Journal of Geotechnical and Geoenvironmental Engineering, ASCE*, 132(2):194–201, 2006.

[32] I. B. Gratchev, K. Sassa, and H. Fukuoka. How Reliable is the plasticity index for estimating the liquefaction potential of clayey sands? *Journal of Geotechnical and Geoenvironmental Engineering, ASCE*, 132(1):124–127, 2006.

[33] J.L.H. Grozic, P.K. Robertson, and N.R. Morgenstern. The behavior of loose gassy sand. *Canadian Geotechnical Journal*, 36(3):482–492, 2000.

[34] S.M. Haeri and M.R. Shakeri. Effects of membrane compliance on pore water pressure generation in gravelly sands under cyclic loading. *Geotechnical Testing Journal, ASTM*, 33(5):1–10, 2010.

[35] J. He, J. Chu, and V. Ivanov. Mitigation of liquefaction of saturated sand using biogas. *Géotechnique*, 63(4):267–275, 2013.

[36] K.-G. Hinzen. The use of engineering seismological models to interpret archaeoseismological findings in Tolbiacum, Germany, a case study. *Bulletin of the Seismological Society of America*, 95:521–539, 2005.

[37] K.-G. Hinzen and S.K. Reamer. Seismicity, seismotectonics, and seismic hazard in the northern Rhine area. In S. Stein and S. Mazzotti, editors, *Continental Intraplate Earthquakes: Science, Hazard, and Policy Issues: Geological Society of America Special Paper 425*, pages 225–242, 2007.

[38] M. Hyodo, A.F.L. Hyde, and N. Aramaki. Liquefaction of crushable soils. *Géotechnique*, 48(4):527–543, 1998.

[39] M. Hyodo, A.F.L. Hyde, N. Aramaki, and Y. Nakata. Undrained monotonic and cyclic shear behaviour of sand under low and high confining stresses. *Soils and Foundations*, 42(3):63–76, 2002.

[40] M. Hyodo, H. Murata, N. Yasufuku, and T. Fujii. Undrained cyclic shear strength and residual shear strain of saturated sand by cyclic triaxial tests. *Soils and Foundations*, 31(3):60–76, 1991.

[41] M. Hyodo, H. Tanimizu, N. Yasufuku, and H. Murata. Undrained cyclic and monotonic triaxial behaviour of saturated loose sand. *Soils and Foundations*, 34(1):19–32, 1994.

[42] K. Ishihara. *Soil Behaviour in Earthquake Geotechnics*. Oxford Science Publications, 1996.

[43] K. Ishihara and J. Koseki. Cyclic shear strength of fines-containing sands, earthquake geotechnical engineering. In *Proceedings of the Discussion Session on Influence of Local Conditions on Seismic Response, 12th ICSMFE Rio de Janeiro*, pages 101–106, 1989.

[44] K. Ishihara and S. Okada. Effects of stress history on cyclic behavior of sand. *Soils and Foundations*, 18(4):31–45, 1978.

[45] K. Ishihara and S. Okada. Yielding of overconsolidated sand and liquefaction model under cyclic stresses. *Soils and Foundations*, 18(1):57–72, 1978.

[46] K. Ishihara and S. Okada. Effects of large preshearing on cyclic behavior of sand. *Soils and Foundations*, 22(3):109–125, 1982.

[47] K. Ishihara, M. Sodekawa, and Y. Tanaka. Effects of overconsolidation on liquefaction characteristics of sands containing fines. *Dynamic Geotechnical Testing, ASTM*, STP 654:246–264, 1978.

[48] K. Ishihara and H. Takatsu. Effects of overconsolidation and K_0 conditions on the liquefaction characteristics of sands. *Soils and Foundations*, 19(4):59–68, 1979.

[49] Y. Jafarian, I. Towhata, M.H. Baziar, A. Noorzad, and A. Bahmanpour. Strain energy based evaluation of liquefaction and residual pore water pressure in sands using cyclic torsional shear experiments. *Soil Dynamics and Earthquake Engineering*, 35:13–28, 2012.

[50] M. Kazama, A. Yamaguchi, and E. Yanagisawa. Liquefaction resistance from a ductility viewpoint. *Soils and Foundations*, 40(6):47–60, 2000.

[51] K. Kegel. *Bergmännische Gebirgsmechanik*. Halle (Saale), 1950.

[52] M. Kiekbusch and B. Schuppener. Membrane penetration and its effects on pore pressure. *Journal of the Geotechnical Engineering Division, ASCE*, 103(GT11):1267–1279, 1977.

[53] T. Kokusho, T. Hara, and R. Hiraoka. Undrained shear strength of granular soils with different particle gradations. *Journal of Geotechnical and Geoenvironmental Engineering, ASCE*, 130(6):621–629, 2004.

[54] J. Koseki, T. Yoshida, and T. Sato. Liquefaction properties of Toyoura sand in cyclic torsional shear tests under low confining stress. *Soils and Foundations*, 45(5):103–113, 2005.

[55] S.L. Kramer. *Geotechnical earthquake engineering*. Prentice-Hall, Upper Saddle River, N.J., 1996.

[56] S.L. Kramer and N. Sivaneswaran. A non-destructive specimen-specific method for measurement of membrane penetration in the triaxial test. *Geotechnical Testing Journal, ASTM*, 12(1):50–59, 1989.

[57] S.L. Kramer and N. Sivaneswaran. Stress-path dependent correction for membrane penetration. *Journal of Geotechnical Engineering, ASCE*, 115(12):1787–1804, 1989.

[58] K. Kuwano, H. Nakazawa, K. Sugihara, and H. Yabe. Undrained cyclic shear strength of sand containing fines (in Japanese). In *Proc. 11th Japan Nat. Conf. Geotech. Eng.*, volume 1, pages 993–994, 1996.

[59] R.S. Ladd. Specimen preparation and liquefaction of sands. *Journal of the Geotechnical Engineering Division, ASCE*, 100(GT10):1180–1184, 1974.

[60] R.S. Ladd. Specimen preparation and cyclic stability of sands. *Journal of the Geotechnical Engineering Division, ASCE*, 103(GT6):535–547, 1977.

[61] R.S. Ladd. Preparing test specimens using undercompaction. *Geotechnical Testing Journal, ASTM*, 1(1):16–23, 1978.

[62] P.V. Lade and S.B. Hernandez. Membrane penetration effects in undrained tests. *Journal of the Geotechnical Engineering Division, ASCE*, 103(GT2):109–125, 1977.

[63] K.L. Lee and J.A. Fitton. Factors affecting the cyclic loading strength of soil. In *Vibration Effects of Earthqakes on Soils and Foundations, ASTM Special Technical Publication 450*, pages 71–95, 1969.

[64] K.L. Lee and J.A. Focht. Liquefaction potential of Ekofisk tank in North Sea. *Journal of the Geotechnical Engineering Division, ASCE*, 101(5):423–438, 1975.

[65] H. Lin and E.T. Selig. An alternative method for determining the membrane penetration correction curve. *Geotechnical Testing Journal, ASTM*, 10(3):151–155, 1987.

[66] S-C.R. Lo, J. Chu, and I.K. Lee. A technique for reducing membrane penetration and bedding errors. *Geotechnical Testing Journal, ASTM*, 12(4):311–316, 1989.

[67] G.R. Martin, W.D.L. Finn, and H.B. Seed. Effects of system compliance on liquefaction tests. *Journal of the Geotechnical Engineering Division, ASCE*, 104(GT4):463–479, 1978.

[68] S. Miura and S. Toki. A sample preparation method and its effect on static and cyclic deformation-strength properties of sand. *Soils and Foundations*, 22(1):61–77, 1982.

[69] F. Molenkamp and H.J. Luger. Modeling and minimization of membrane penetration effects in tests on granular soils. *Géotechnique*, 31(4):471–486, 1981.

[70] J. Montgomery, R.W. Boulanger, and L.F. Harder. Examination of the K_σ overburden correction factor on liquefaction resistance. *Journal of Geotechnical and Geoenvironmental Engineering, ASCE*, 2014.

[71] J.P. Mulilis, C.K. Chan, and H.B. Seed. The effects of method of sample preparation on the cyclic stress-strain behavior of sands. Technical Report EERC 75-18, Earthquake Engineering Research Center, University of California, Berkeley, 1975.

[72] J.P. Mulilis, H.B. Seed, C.K. Chan, J.K. Mitchell, and K. Arulanandan. Effects of sample preparation on sand liquefaction. *Journal of the Geotechnical Engineering Division, ASCE*, 103(GT2):91–108, 1977.

[73] P.L. Newland and B.H. Alley. Volume changes during drained triaxial tests on granular materials. *Géotechnique*, 7(1):17–34, 1957.

[74] P.L. Newland and B.H. Alley. Volume changes during undrained triaxial tests on saturated dilatant granular materials. *Géotechnique*, 9(3):174–182, 1959.

[75] P.G. Nicholson, R.B. Seed, and H.A. Anwar. Elimination of membrane compliance in undrained triaxial testing. I. Measurement and evaluation. *Canadian Geotechnical Journal*, 30(5):727–738, 1993.

[76] M. Oda, K. Kawamoto, K. Suzuki, H. Fujimori, and M. Sato. Microstructural interpretation on reliquefaction of saturated granular soils under cyclic loading. *Journal of Geotechnical and Geoenvironmental Engineering, ASCE*, 127(5):416–423, 2001.

[77] S. Ohara and T. Yamamoto. A practical method for obtaining correction factor of liquefaction resistance for membrane penetration. *Soils and Foundations*, 31(2):188–196, 1991.

[78] M. Okamura and Y. Soga. Effects of pore fluid compressibility on liquefaction resistance of partially saturated sand. *Soils and Foundations*, 46(5):695–700, 2006.

[79] M. Okamura, M. Takebayashi, K. Nishida, N. Fujii, M. Jinguji, T. Imasato, H. Yasuhara, and E. Nakagawa. In-situ desaturation test by air injection and its evaluation through field monitoring and multiphase flow simulation. *Journal of Geotechnical and Geoenvironmental Engineering, ASCE*, 137(7):643–652, 2011.

[80] R. P. Orense, N. Yoshimoto, and M. Hyodo. Cyclic shear behavior and seismic response of partially saturated slopes. *Soil Dynamics and Earthquake Engineering*, 42(6):71–79, 2012.

[81] A. Papadopoulou and T. Tika. The effect of fines on critical state and liquefaction resistance characteristics of non-plastic silty sands. *Soils and Foundations*, 48(5):713–725, 2008.

[82] S.-S. Park and Y.-S. Kim. Liquefaction resistance of sands containing plastic fines with different plasticity. *Journal of Geotechnical and Geoenvironmental Engineering, ASCE*, 139(5):825–830, 2013.

[83] T. Park and M.L. Silver. Dynamic soil properties required to predict the dynamic behavior of elevated transportation structures. Technical Report DOT-TST-75-44, U.S. Dept. of Transportation, 1975.

[84] R. Petri, W. Stein, D. Dahmen, and K. Buschhüter. Sustainable follow-up use of recultivated surfaces. Evaluation of residual lakes and high dumps in the Rhenish lignite-mining area after the end of mining supervison. *World of Mining*, 65(2):92–101, 2013.

[85] D. Porcino, G. Caridi, and V.N. Ghionna. Undrained monotonic and cyclic simple shear behaviour of carbonate sand. *Géotechnique*, 58(8):635–644, 2008.

[86] D. Porcino, G. Cicciù, and V.N. Ghionna. Laboratory investigation of the undrained cyclic behaviour of a natural coarse sand from undisturbed and reconstituted samples. In T. Triantafyllidis, editor, *Cyclic Behaviour of Soils and Liquefaction Phenomena, Proc. of CBS04*, pages 187–192. Balkema, 2004.

[87] K.S. Prakasha and V.S. Chandrasekaran. Behavior of marine sand-clay mixtures under static and cyclic triaxial shear. *Journal of Geotechnical and Geoenvironmental Engineering, ASCE*, 131(2):213–222, 2005.

[88] N.S. Rad, A.J.D. Vianna, and T. Berre. Gas in soils. II - Effect of gas on undrained static and cyclic strength of sand. *Journal of Geotechnical Engineering, ASCE*, 120(4):716–736, 1994.

[89] V.S. Raju and S.K. Sadasivian. Membrane penetration in triaxial tests on sand. *Journal of the Geotechnical Engineering Division, ASCE*, 100(GT4):482–489, 1974.

[90] K.V. Ramana and V.S. Raju. Membrane penetration in triaxial tests. *Journal of Geotechnical Engineering, ASCE*, 108(2):305–310, 1982.

[91] K.M. Rollins and H.B. Seed. Influence of buildings on potential liquefaction damage. *Journal of Geotechnical Engineering, ASCE*, 116(2):165–185, 1990.

[92] G.A. Ross, H.B. Seed, and R.R. Migliaccio. Bridge foundations in Alaska earthquake. *Journal of the Soil Mechanics and Foundations Division, ASCE*, 95(SM4):1007–1036, 1969.

[93] K. Sassa, G. Wang, H. Fukuoka, and D.A. Vankov. Shear-displacement-amplitude dependent pore-pressure generation in undrained cyclic loading ring shear tests - An energy approach. *Journal of Geotechnical and Geoenvironmental Engineering, ASCE*, 131(6):750–761, 2005.

[94] K. Schmidtalbers. Meßtechnische Untersuchungen des Betriebsablaufes während der Schüttungsperiode von Halden über deren inneren Aufbau. Dissertation, TU Clausthal, 1969.

[95] H.B. Seed and I.M. Idriss. Simplified procedure for evaluating soil liquefaction potential. *Journal of the Soil Mechanics and Foundations Division, ASCE*, 97(SM9):1249–1273, 1971.

[96] H.B. Seed, K. Mori, and C.K. Chan. Influence of seismic history on liquefaction of sands. *Journal of the Geotechnical Engineering Division, ASCE*, 103(GT4):257–270, 1977.

[97] H.B. Seed and W.H. Peacock. Test procedures for measuring soil liquefaction characteristics. *Journal of the Soil Mechanics and Foundations Division, ASCE*, 97(SM8):1099–1119, 1971.

[98] R.B. Seed and L.F. Harder. SPT-based analysis of cyclic pore pressure generation and undrained residual strength. In *Proceedings of the B. Seed Memorial Symposium*, volume 2, pages 351–376, 1990.

[99] R.B. Seed, S.R. Lee, and H.-L. Jong. Penetration and liquefaction resistances: prior seismic history effects. *Journal of Geotechnical Engineering, ASCE*, 114(6):691–697, 1988.

[100] S.S. Sharma and M. Ismail. Monotonic and cyclic behavior of two calcareous soils of different origins. *Journal of Geotechnical and Geoenvironmental Engineering, ASCE*, 132(12):1581–1591, 2006.

[101] M. Sherif, I. Ishibashi, and C. Tsuchiya. Saturation effects on initial soil liquefaction. *Journal of the Geotechnical Engineering Division, ASCE*, 103(GT8):914–917, 1977.

[102] M.L. Silver, C.K. Chan, R.S. Ladd, K.L. Lee, D.A. Tiedemann, F.C. Townsend, J.E. Valera, and J.H. Wilson. Cyclic triaxial strength of standard test sand. *Journal of the Geotechnical Engineering Division, ASCE*, 102(GT5):511–523, 1976.

[103] M.L. Silver and T.K. Park. Liquefaction potential evaluated from cyclic strain-controlled properties tests on sands. *Soils and Foundations*, 16(3):51–65, 1976.

[104] S. Sivathayalan and D. Ha. Effect of static shear stress on the cyclic resistance of sands in simple shear loading. *Canadian Geotechnical Journal*, 48:1471–1484, 2011.

[105] S. Sivathayalan and Y.P. Vaid. Truly undrained response of granular soils with no membrane-penetration effects. *Canadian Geotechnical Journal*, 35(5):730–739, 1998.

[106] A.W. Skempton. The pore pressure coefficients A and B. *Géotechnique*, 4(4):143–147, 1954.

[107] C.A. Stamatopoulos. Discussion of "The effect of fines on critical state and liquefaction resistance characteristics of non-plastic silty sands" by Papadopoulou & Tika. *Soils and Foundations*, 50(1):173–176, 2010.

[108] T. Suzuki and S. Toki. Effects of preshearing on liquefaction characteristics of saturated sand subjected to cyclic loading. *Soils and Foundations*, 24(2):16–28, 1984.

[109] H.Y. Sze and J. Yang. Failure modes of sand in undrained cyclic loading: Impact of sample preparation. *Journal of Geotechnical and Geoenvironmental Engineering, ASCE*, 140(1):152–169, 2014.

[110] F. Tatsuoka, H. Kimura, and T.B.S. Pradhan. Liquefaction strength of sands subjected to sustained pressure. *Soils and Foundations*, 28(1):119–131, 1988.

[111] F. Tatsuoka, K. Ochi, S. Fujii, and M. Okamoto. Cyclic undrained triaxial and torsional shear strength of sands for different sample preparation methods. *Soils and Foundations*, 26(3):23–41, 1986.

[112] F. Tatsuoka, S. Toki, S. Miura, H. Kato, M. Okamoto, S.-I. Yamada, S. Yasuda, and F. Tanizawa. Some factors affecting cyclic undrained triaxial strength of sand. *Soils and Foundations*, 26(3):99–116, 1986.

[113] S. Teachavorasinskun, F. Tatsuoka, and D.C.F. Lo Presti. Effects of cyclic prestraining on dilatancy characteristics and liquefaction of sand. In Shibuya, Mitachi, and Miura, editors, *Pre-failure deformation of geomaterials*, pages 75–80, 1994.

[114] K. Tokimatsu. System compliance correction from pore pressure response in undrained triaxial tests. *Soils and Foundations*, 30(2):14–22, 1990.

[115] K. Tokimatsu and K. Nakamura. A liquefaction test without membrane penetration effects. *Soils and Foundations*, 26(4):127–138, 1986.

[116] K. Tokimatsu and K. Nakamura. A simplified correction for membrane compliance in liquefaction tests. *Soils and Foundations*, 27(4):111–122, 1987.

[117] I. Towhata. *Geotechnical Earthquake Engineering*. Springer, 2008.

[118] Y. Tsukamoto, K. Ishihara, H. Nakazawa, K. Kamada, and Y. Huang. Resistance of partly saturated sand to liquefaction with reference to longitudinal and shear wave velocities. *Soils and Foundations*, 42(6):93–104, 2002.

[119] T. Unno, M. Kazama, R. Uzuoka, and N. Sento. Liquefaction of unsaturated sand considering the pore air pressure and volume compressibility of the soil particle skeleton. *Soils and Foundations*, 48(1):87–99, 2008.

[120] Y. Vaid and W.D.L. Finn. Static shear and liquefaction potential. *Journal of the Geotechnical Engineering Division, ASCE*, 105(GT10):1233–1246, 1979.

[121] Y.P. Vaid and J.C. Chern. Cyclic and monotonic undrained response of sands. In *Proceedings of Advances in the Art of Testing Soils under Cyclic Loading Conditions, Detroit*, pages 120–147, 1985.

[122] Y.P. Vaid, E.K.F. Chung, and R.H. Kuerbis. Preshearing and undrained response of sands. *Soils and Foundations*, 29(4):49–61, 1989.

[123] Y.P. Vaid, J.M. Fisher, R.H. Kuerbis, and D. Negussey. Particle gradation and liquefaction. *Journal of Geotechnical Engineering, ASCE*, 116(4):698–703, 1990.

[124] Y.P. Vaid and D. Negussey. A critical assessment of membrane penetration in the triaxial test. *Geotechnical Testing Journal, ASTM*, 7(2):70–76, 1984.

[125] Y.P. Vaid and S. Sivathayalan. Static and cyclic liquefaction potential of Fraser Delta sand in simple shear and triaxial tests. *Canadian Geotechnical Journal*, 33:281–289, 1996.

[126] Y.P. Vaid and S. Sivathayalan. Fundamental factors affecting liquefaction susceptibility of sands. *Canadian Geotechnical Journal*, 37:592–606, 2000.

[127] Y.P. Vaid and J. Thomas. Post liquefaction behaviour of sand. In *Proceedings of the 13th International Conference on Soil Mechanics and Foundation Engineering, New Delhi*, volume 1, pages 1303–1310, 1994.

[128] Y.P. Vaid and J. Thomas. Liquefaction and postliquefaction behavior of sand. *Journal of Geotechnical Engineering, ASCE*, 121(2):163–173, 1995.

[129] C.A. Vega-Posada, R.J. Finno, and D.G. Zapata-Medina. Effect of gas on the mechanical behavior of medium-dense sands. *Journal of Geotechnical and Geoenvironmental Engineering, ASCE*, 2014.

[130] T. Wichtmann. Soil behaviour under cyclic loading - experimental observations, constitutive description and applications. Habilitation thesis, Publications of the Institute of Soil Mechanics and Rock Mechanics, Karlsruhe Institute of Technology, Issue No. 181, 2016.

[131] T. Wichtmann, W. Fuentes, and Th. Triantafyllidis. Inspection of three sophisticated constitutive models based on monotonic and cyclic tests on fine sand: Hypoplasticity vs. Sanisand vs. ISA. *Soil Dynamics and Earthquake Engineering (submitted)*, 2018.

[132] T. Wichtmann, A. Niemunis, Th. Triantafyllidis, and M. Poblete. Correlation of cyclic preloading with the liquefaction resistance. *Soil Dynamics and Earthquake Engineering*, 25(12):923–932, 2005.

[133] T. Wichtmann and Th. Triantafyllidis. An experimental data base for the development, calibration and verification of constitutive models for sand with focus to cyclic loading. Part I: Tests with monotonic loading and stress cycles. *Acta Geotechnica*, 11(4):739–761, 2016.

[134] T. Wichtmann and Th. Triantafyllidis. An experimental data base for the development, calibration and verification of constitutive models for sand with focus to cyclic loading. Part II: tests with strain cycles and combined cyclic and monotonic loading. *Acta Geotechnica*, 11(4):763–774, 2016.

[135] D. Wijewickreme, S. Sriskandakumar, and P. Byrne. Cyclic loading response of loose air-pluviated Fraser River sand for validation of numerical models simulating centrifuge tests. *Canadian Geotechnical Journal*, 42:550–561, 2005.

[136] H. Xia and T. Hu. Effects of saturation and back pressure on sand liquefaction. *Journal of Geotechnical Engineering, ASCE*, 117(9):1347–1362, 1991.

[137] S. Yamashita and S. Toki. Effects of fabric anisotropy of sand on cyclic undrained triaxial and torsional strengths. *Soils and Foundations*, 33(3):92–104, 1993.

[138] J. Yang. Liquefaction resistance of sand in relation to P-wave velocity. *Géotechnique*, 52(4):295–298, 2002.

[139] J. Yang. Pore pressure coefficient for soil and rock and its relation to compressional wave velocity. *Géotechnique*, 55(3):251–256, 2005.

[140] J. Yang, S. Savidis, and M. Roemer. Evaluating liquefaction strength of partially saturated sand. *Journal of Geotechnical and Geoenvironmental Engineering, ASCE*, 130(9):975–979, 2004.

[141] J. Yang and H.Y. Sze. Cyclic behaviour and resistance of saturated sand under non-symmetrical loading conditions. *Géotechnique*, 61(1):59–73, 2011.

[142] J. Yang and H.Y. Sze. Cyclic strength of sand under sustained shear stress. *Journal of Geotechnical and Geoenvironmental Engineering, ASCE*, 137(12):1275–1285, 2011.

[143] M. K. Yegian, E. Eseller-Bayat, A. Alshawabkeh, and S. Ali. Induced-partial saturation for liquefaction mitigation: Experimental investigation. *Journal of Geotechnical and Geoenvironmental Engineering, ASCE*, 133(4):372–382, 2007.

[144] Y. Yoshimi and H. Oh-Oka. Influence of degree of shear stress reversal on the liquefaction potential of saturated sand. *Soils and Foundations*, 15(3):27–40, 1975.

[145] Y. Yoshimi, K. Tanaka, and K. Tokimatsu. Liquefaction resistance of a partially saturated sand. *Soils and Foundations*, 29:157–162, 1989.

[146] Y. Yoshimi, K. Tokimatsu, and Y. Hosaka. Evaluation of liquefaction resistance of clean sands based on high-quality undisturbed samples. *Soils and Foundations*, 29:93–104, 1989.

[147] Y. Yoshimi, K. Tokimatsu, O. Kaneko, and Y. Makihara. Undrained cyclic shear strength of a dense Niigata sand. *Soils and Foundations*, 24(4):131–145, 1984.